JOURNAL OF GEOPHYSICAL RESEARCH, VOL. 93, NO. D2, PAGES 1431–1451, FEBRUARY 20, 1988

Tropospheric Ozone and Aerosol Distributions Across the Amazon Basin

E. V. BROWELL, G. L. GREGORY, AND R. C. HARRISS

Atmospheric Sciences Division, NASA Langley Research Center, Hampton, Virginia

V. W. J. H. KIRCHHOFF

Instituto de Pesquisas Espaciais, São Jose dos Campos, São Paulo, Brazil

Ozone and aerosol distributions were measured during July–August 1985 over the tropical rain forest of Brazil as part of the NASA Global Tropospheric Experiment to study the Amazon boundary layer. Remote and in situ measurements of O_3 and aerosols were made from a NASA Electra aircraft on several long-range flights spanning different areas between Tabatinga and Belem, Brazil. Continuous O_3 distributions were obtained between the aircraft altitude and the ground with an airborne differential absorption lidar (DIAL) system. Aerosol distributions were also continuously measured above and below the aircraft with the DIAL system. In situ O_3 measurements were made on the aircraft and from ground-launched ozonesondes at Manaus and Natal. Large-scale variations in the vertical and horizontal distributions of O_3 and aerosols were observed on nearly all flights over the Amazon Basin, with O_3 exceeding 50 parts per billion by volume (ppbv) in some regions. Both positive and negative correlations were observed between O_3 mixing ratios and aerosol concentrations. In nearly all cases, when O_3 and aerosols were negatively correlated, this represented clean midtropospheric air, and when they were positively correlated, the air mass had undergone photochemical O_3 production as a result of biomass burning. A 59% increase in the planetary boundary layer (PBL) O_3 level was observed between the initial Manaus-Belem flights on July 23–24, 1985 and the later flights on August 8–9, 1985. This was attributed to the increase in biomass burning near the Rio Amazonas and its tributaries and in savannah regions south of the Amazon Basin. Flights to the west of Manaus measured enhanced O_3 and aerosol levels near the Rio Solimões, while the area sampled upwind of the river exhibited lower O_3 levels. This was explained by the increased incidence of biomass burning near the river. This paper also examines the variability of the trade wind inversion (TWI) height across the Amazon Basin and the influence of O_3 levels above the TWI on the budget of O_3 in the PBL. Measurements reported for the early dry season characterize the background distribution of O_3 and aerosols in the PBL prior to the onset of extensive biomass burning. These data provide the basis for a basin-scale estimate of photochemical O_3 production from biomass-burning emissions.

INTRODUCTION

Recent studies by *Crutzen et al.* [1985] suggest that three processes may be particularly important in determining O_3 distributions over the central Amazon during the dry season: (1) photochemical production of O_3 associated with biomass burning, (2) O_3 destruction in the boundary layer over the rain forest by reactions with isoprene (C_5H_8) and other hydrocarbons, and (3) dry deposition on the forest canopy. Much of the biomass burning takes place in the savannah region south of the Amazon, with subsequent long-range transport to the Amazon Basin in the mid-troposphere [*Fishman et al.*, 1986]. We also know from the work of numerous investigators (see, for example, *Garstang et al.* [this issue]) that thunderstorms can cause downward transport of O_3 from the reservoir layer in the upper troposphere into the planetary boundary layer (PBL). This complex interaction of source and sink processes can result in large variability for both vertical and horizontal O_3 distributions, as observed by *Delany et al.* [1985] over Brazil during the dry season. In this paper we examine the spatial and temporal variability of O_3 across the Amazon Basin during July–August 1985 and relate these results to the various sources and sinks for O_3 in the PBL.

Paper number 7D0707.
0148-0227/88/007D-0707$05.00

Knowledge of atmospheric dynamics and structure is essential for proper sampling of O_3 and for interpretation of remote and in situ measurements of gases and aerosols. The distribution of aerosols over the tropical rain forest provides important information on mixed layer heights, trade wind inversion heights, location and depth of stable layers, and cloud characteristics. In addition to their use as a tracer of dynamics and atmospheric structure, aerosols can provide information on the history or source of an air mass. In general, the free troposphere has less aerosol loading than does the PBL, and a plume from a fire has significantly more aerosols than does the ambient air surrounding the fire. The aerosol distributions obtained in this study provide the information needed to define the atmospheric structure and to interpret the O_3 data.

During July–August 1985 an extensive field experiment was conducted over the tropical rain forest of Brazil to investigate chemical and transport processes controlling the composition of the lower troposphere during the "dry" season [*Harriss et al.*, this issue]. This experiment was the second in a series of NASA Global Tropospheric Experiments (GTE) to focus on important biogeochemical systems that could play a significant role in influencing global budgets of gases and aerosols in the troposphere. The Amazon Basin represented an ideal location to study the background conditions for sources and sinks of gases and aerosols over a tropical rain forest, since it represents the largest single area of this kind anywhere in the world. Rain forest and tropical

savannah regions account for a significant fraction of the world's biomass, and biogeochemical cycling rates are high relative to other ecosystems. For example, tropical rain forests constitute 6.6% of the Earth's terrestrial surface area and contribute over 17% of global net primary production [*Ajtay et al.*, 1979]. Model calculations [e.g., *Crutzen and Gidel*, 1983] and preliminary field measurements [e.g., *Delany et al.*, 1985] have indicated a major role for the tropics in global tropospheric chemistry. The natural emissions of NO_x, NMHC, CH_4, and CO from these areas and their transport into the PBL and free troposphere can have an impact on the global O_3 budget in the troposphere as a result of photochemical processes. In addition, dry deposition of O_3 on the foliage of the rain forest can be an effective removal process [see *Kirchhoff*, this issue]. Burning in the savannah and portions of the rain forest increases with the lengthening dry season, and the products of biomass burning can result in photochemical production of O_3 [*Delany et al.*, 1985]. While the impact of biomass burning was not the focus of the Amazon Boundary Layer Experiment (ABLE 2A), the contribution of the products from these fires to the composition of the PBL across the Amazon Basin during the experiment had to be evaluated because of the extent of the burning encountered.

This paper discusses the O_3 and aerosol data obtained across the Amazon Basin from July 18 to August 9, 1985, as part of the NASA GTE/ABLE 2A field experiment. Flights were conducted from Tabatinga (4°S, 70°W) to Belem (1°S, 50°W) in a NASA Electra aircraft, with its base of operations at Manaus (3°S, 60°W). Airborne O_3 measurements were made in situ and with a lidar system pointed below the aircraft in a nadir mode of operation. Ozonesondes were launched from near Manaus to investigate O_3 distributions to the tropopause. Aerosol distributions were measured in situ on the aircraft and above and below the aircraft with the lidar system. This paper emphasizes the distribution of O_3 and aerosols between the top of the mixed layer and the trade wind inversion (TWI). Companion papers in this issue discuss the temporal and spatial variability of O_3 in the mixed layer above the forest canopy [*Gregory et al.*, this issue], and in the free troposphere above Manaus (V. W. J. H. Kirchhoff, E. V. Browell, and G. L. Gregory, Ozone profile measurements in Amazonia, submitted to the *Journal of Geophysical Research*, 1987; hereafter Kirchhoff et al., submitted manuscript, 1987). Here we discuss the positive and negative correlations found between O_3 and aerosols and how this relationship helps to track a particular air mass and to determine its origin. The spatial and temporal variation of O_3 in the PBL across the Amazon Basin is discussed with respect to the height of the TWI, gradients in O_3 above the TWI, the depth of the mixed layer, and biomass burning. The spatial and temporal variation of aerosols is discussed to establish the atmospheric structure, dynamics, and aerosol distribution encountered across the Amazon Basin. Data on temperature, dew point, and winds are included when necessary to support the O_3 and aerosol analysis, and discussion of the data on other species is found in companion papers in this issue.

AIRBORNE LIDAR AND IN SITU INSTRUMENTATION

The remote measurement of O_3 and aerosol distributions along the aircraft ground track is provided by the airborne differential absorption lidar (DIAL) system [*Browell et al.*, 1983]. This lidar system can provide O_3 profiles along its line of sight, and, when operated in a nadir mode from an aircraft during the daytime, mixing ratios of O_3 can be measured over a 5-km range with an accuracy of $\leq$10% and a vertical and horizontal resolution of 210 m and 6 km (300 laser shots), respectively [*Browell*, 1983; *Browell et al.*, 1983; 1985*a*]. Data from this system have been used in several studies of tropospheric O_3 [*Shipley et al.*, 1984; *Browell et al.*, 1985*b*; *Fishman et al.*, 1985; *Vukovich et al.*, 1985; *Ching et al.*, 1987] and in a recent study of tropopause fold structure [*Browell et al.*, 1987]. The two laser pulses used in the DIAL measurement of O_3 in this study are independently tuned, with one pulse set to a wavelength that is strongly absorbed by O_3 (286 nm) and the other set to a wavelength that is only slightly absorbed by O_3 (300 nm). The output pulses are transmitted simultaneously in a traditional lidar mode to obtain range-dependent information at two wavelengths. The relative differences between the two lidar signals at any two ranges are predominantly due to the absorption of O_3, which can then be related to the concentration of O_3 between the two ranges. An O_3 profile can then be derived by calculating the absorption over 210-m range intervals along the UV lidar returns. Additional details on the airborne DIAL system and the techniques used in the DIAL O_3 data reduction are discussed by *Browell et al.* [1983; 1985*a*]. Airborne lidar data are obtained at a 5-Hz rate, which represents a lidar profile with a vertical and horizontal resolution of 15 and 20 m, respectively. These data are averaged vertically and horizontally to reduce the DIAL O_3 measurement statistics. Increasing the number of shots averaged and/or the vertical resolution beyond the levels used in this study can further increase the DIAL measurement accuracy and range.

Laser pulses at 1064 nm were also transmitted in a nadir and zenith mode from the aircraft along with the DIAL wavelengths at 286 and 300 nm in the nadir mode. The lidar returns at 1064 nm were used to investigate the aerosol/cloud distributions below and above the aircraft. These measurements were also made at a 5-Hz rate; however, because of the better statistics involved in the measurement of aerosol distributions, the vertical and horizontal resolution of the measurement could be as small as that defined by the pulse rate and data digitization, or 15 and 20 m, respectively. The use of lidar returns at 1064 nm provides good contrast between molecular and aerosol backscattering and less atmospheric attenuation than at shorter wavelengths. This results in more sensitive detection of atmospheric aerosol distributions along the lidar line of sight. Continuous color plots of aerosol profiles along the aircraft ground track were obtained from either the nadir or zenith lidar channels in real time on the aircraft for selection of aircraft sampling altitudes or spiral locations.

Two chemiluminescence O_3 systems were used for continuous, in situ measurements on the aircraft [*Gregory et al.*, 1983]. The in situ O_3 data used in this study were from a NO chemiluminescence instrument which has an O_3 mixing ratio measurement accuracy of 5 parts per billion by volume (ppbv) or 5% (whichever is largest) with a 0.20-s response time. Aerosol number densities were measured by a forward scattering spectrometer probe (FSSP). The FSSP counts and sizes aerosols in diameter ranges from 0.5 to 7.5 μm in increments of 0.5 μm, with a counting period which is

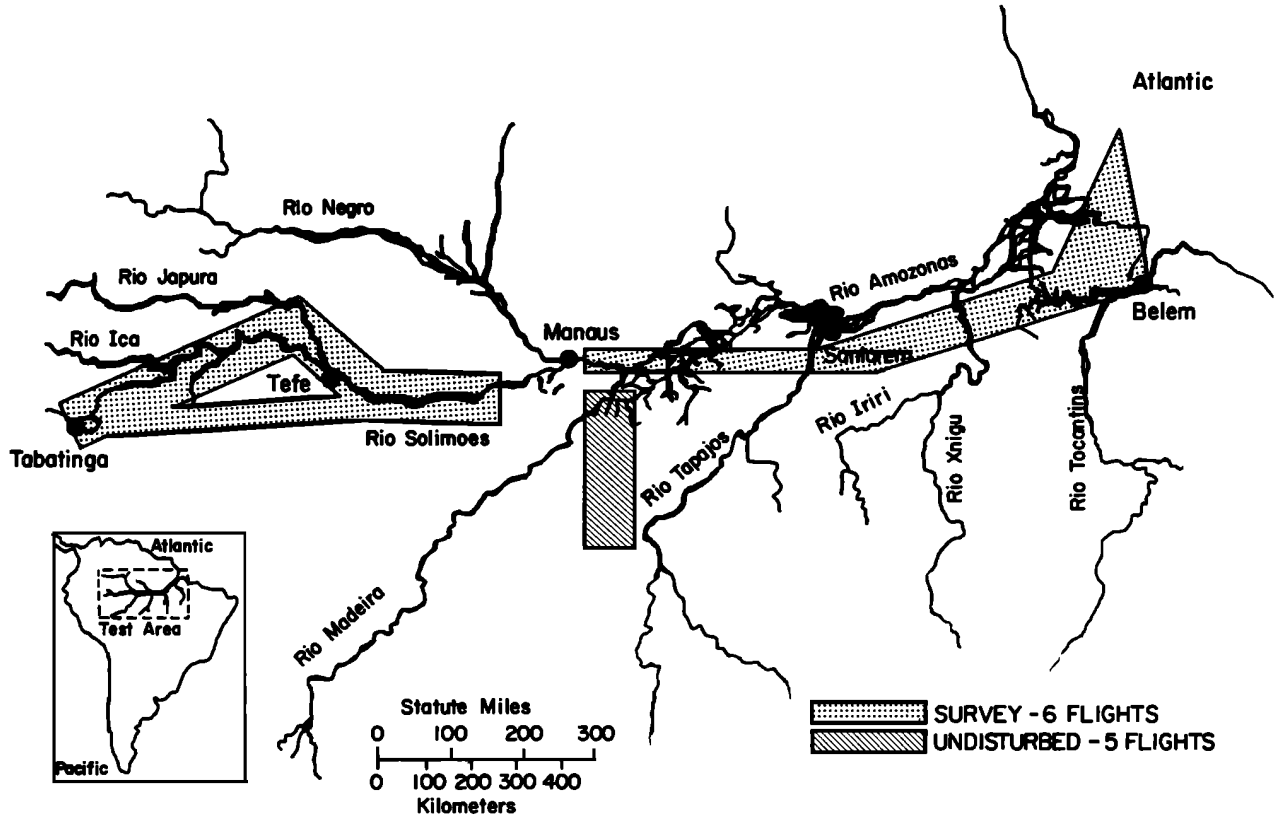

Fig. 1. Map of regions investigated on undisturbed and survey missions during the GTE/ABLE 2A field experiment.

selectable in flight and typically ranges from 10 to 90 s. Total air temperature was measured on the aircraft with a platinum resistance probe. The probe has a measurement accuracy of ±0.5°C and a response time of 1 s. Dew-point temperature was determined with a cooled-mirror hygrometer, which has a measurement accuracy of ±0.2°C and a response time of 2°C s^{-1}. The measurements of temperature and dew point provide information on the thermodynamic properties and identification of layers in the atmosphere.

The NASA Wallops Flight Center Electra aircraft was used as the platform for all flights in this field experiment. It has a nominal air speed of 120 m s^{-1} and a flight endurance of 6.5 hours. The ceiling for this aircraft is about 9 km; however, these experiments did not require flight altitudes above 5 km. In addition to the airborne lidar and instruments for in situ measurements of O_3, aerosol number density and size distribution, temperature, and dew point, the Electra had instrumentation on board for in situ measurements of NO_x, CO, CO_2, CH_4, N_2O, NMHC, sulfur gases, and aerosol composition. A general description of these systems and measurements is given by *Harriss et al.* [this issue], and more details are provided in the other papers in this issue.

Data Results and Discussion

Ozone and aerosol data used in this study were obtained on 11 flights over the Amazon Basin between July 18 and August 9, 1985. The locations of these flights are shown in Figure 1, and a list of the flights is given in Table 1. There were five undisturbed boundary layer investigations that were centered about 250 km southeast of Manaus. These

TABLE 1. Summary of Flights

Date (1985)	Mission Type	Flight Times,* UT		Flight Altitude Range, km
		Takeoff	Landing	
July 18	undisturbed boundary layer (day)	1310	1839	0.2–5.6
July 19	undisturbed boundary layer (day)	1200	1802	0.2–4.7
July 21	undisturbed boundary layer (day)	1058	1701	0.2–4.4
July 23	Manaus to Belem survey	1154	1802	0.2–3.8
July 24	Belem to Manaus survey	1200	1825	0.2–4.4
July 25†	undisturbed boundary layer (night)	1957	0545	0.3–3.8
July 26†	undisturbed boundary layer (night)	2220	0418	0.3–5.3
August 5	Tefe to Tabatinga and return survey	1122	2128	0.2–3.8
August 6	Manaus to Tefe and return survey	1150	1802	0.2–4.1
August 8	Manaus to Belem survey	1150	1757	0.2–4.7
August 9	Belem to Manaus survey	1235	1829	0.2–4.4

* Universal time or GMT is equal to Manaus time plus 4 hours.
† Takeoff date.

flights involved repeated flights between fixed locations at altitudes of 150–5600 m above sea level (ASL). The daytime undisturbed boundary layer experiments generally started soon after sunrise and continued into the early afternoon. This provided an opportunity to investigate the temporal development of the chemistry and dynamics of the mixed layer over the rain forest. The nighttime flights were conducted from the late afternoon to after midnight over the same area as the daytime flights. This permitted the study of the formation of a shallow nocturnal mixed layer over the rain forest and the chemistry and structure of the residual air beneath the TWI in the old PBL. The survey missions included two round-trip flights between Manaus and Belem, separated by 16 days, and round-trip flights between Tefe and Tabatinga and between Manaus and Tefe. The survey missions were composed of a series of high-altitude (3.8–4.7 km) and low-altitude (150 m) legs, which were 75–200 km in length. Details of all the flights conducted in the ABLE 2A field experiment are given by *Harriss et al.* [this issue].

Undisturbed Boundary Layer

Cross sections of aerosol and O_3 distributions observed in the undisturbed daytime case on July 19, 1985, are shown in Plate 1. False color displays of the relative aerosol-backscattering and O_3 mixing ratio distributions are shown along the aircraft flight track. These displays were generated from the airborne lidar data, with the lidar system operating in a nadir mode from an altitude of 4.7 km. The top display is the aerosol distribution derived from the 1064-nm lidar data, with each vertical line representing the average of 15 lidar returns. The solar background and range-squared dependence of the lidar signal were removed prior to producing this display, and because of the high-visibility conditions that existed throughout the experiment, no correction for atmospheric attenuation was needed in the analysis. The top of the forest canopy can be seen as a black line at the bottom of the display. The mixed layer can be readily identified by the enhanced backscattering that extends above the topography to an altitude of about 1500 m near point B and about 1000 m near point A. This results from the mixed layer containing a naturally higher concentration of aerosols compared to the regions above it. Convective plumes resulting from surface heating effects can be seen at the top of the mixed layer, and there is a noticeable variation in the height of the mixed layer from point B to point A. Part of this variation may be due to the additional underlying water associated with flood-plain swamps near point A that reduces surface heating and retards the growth rate of the mixed layer. The black areas at the top of the mixed layer are clouds in various stages of development. The clouds that are optically thick for the lidar have shadows (shown as white areas) beneath them. Because of the release of latent heat in clouds and localized regions of enhanced surface heating and water vapor, some of the clouds have enough buoyancy for them to penetrate the inversion at the top of the mixed layer and ascend to another higher stable level.

The area that is predominantly blue in the aerosol display is the old PBL. This is the region that underwent active mixing by clouds on the preceding day. Under these background undisturbed conditions, the aerosol loading in the PBL is about 50% that in the mixed layer. The inhomogeneity in vertical transport of aerosols and gases, which naturally accompanies mixing by clouds, can be seen in the lidar aerosol display. With the exception of deep convective events, most of the fair-weather cumulus clouds that penetrate the mixed layer inversion into the PBL, which is also called the convective cloud layer (CCL), do not have enough energy to penetrate the inversion at the top of the PBL, which coincides with the TWI. The TWI prevents most of the aerosols and gases from being mixed vertically into the free troposphere. This inversion height can be seen at the altitude where the PBL aerosol loading decreases abruptly to about 40% the value in the PBL (or 20% of the mixed layer value). The average height of the TWI on July 19 was estimated to be at about 3200 m. Temperature and dew-point data obtained near point B are shown next to the aerosol plot for comparison. While it is sometimes difficult to detect the location of an inversion from a temperature plot alone, the dew-point temperature can provide additional insight because of the drying that is usually seen above an inversion. This drying effect is readily seen in this case at the top of the mixed layer and at the TWI. Because of the horizontal variability in the mixing depth and TWI heights, we use values derived for these parameters from the nadir or zenith lidar aerosol data. The TWI heights derived from the lidar data were compared to the temperature and dew-point data to insure they were interpreted correctly.

The O_3 mixing ratio distribution shown at the bottom of Plate 1 was derived from the airborne lidar system with the DIAL technique. Each vertical line represents the average of 300 lidar returns (1-min average or about 7-km horizontal distance), with a vertical resolution of 210 m. A horizontal running average was used to present a continuous O_3 plot that was in phase with the aerosol data. The start of the lidar data begins about 750 m below and above the aircraft, and as a result of the 210-m vertical smoothing of the DIAL data, O_3 calculations are not made within about 300 m of the surface. White areas in the O_3 data represent data gaps due to clouds, when they limit the O_3 retrieval to less than 50% of the horizontal averaging interval. The O_3 distribution across the leg is horizontally homogeneous, with lower O_3 mixing ratios in the mixed layer compared to those in the PBL, which are also lower than those in the free troposphere. An average O_3 profile derived from the lidar data along leg B-A is shown beside the O_3 color plot. The average O_3 mixing ratio in the mixed layer was found to be about 21 ppbv, and it increased slowly in the PBL to 26 ppbv at the TWI. The vertical gradient of O_3 between the mixed layer and the TWI was 2.8 ppbv km^{-1}, and above the TWI, the O_3 levels increased rapidly into the free troposphere. This trend in the O_3 distribution is negatively correlated with the aerosol distribution and supports the theory that in the undisturbed and unpolluted atmosphere over the tropical rain forest, the predominant source of O_3 in the mixed layer and PBL results from downward transport of O_3 from the free troposphere, with destruction of O_3 at the surface. An intriguing, albeit limited, set of observations of the undisturbed, unpolluted mixed layer over the rain forest indicate evidence for natural photochemical production of O_3. The "patches" of high O_3 (30–40 ppbv) in the daytime mixed layer shown in Plate 1 are not associated with any observed biomass burning. Carbon monoxide concentrations in this mixed layer were at minimum observed levels of 75–80 ppbv [*Sachse et al.*, this issue], indicating unpolluted conditions, and NO concentrations were 15–35 parts per trillion by volume (pptv), which is sufficient to result in O_3 production during isoprene oxida-

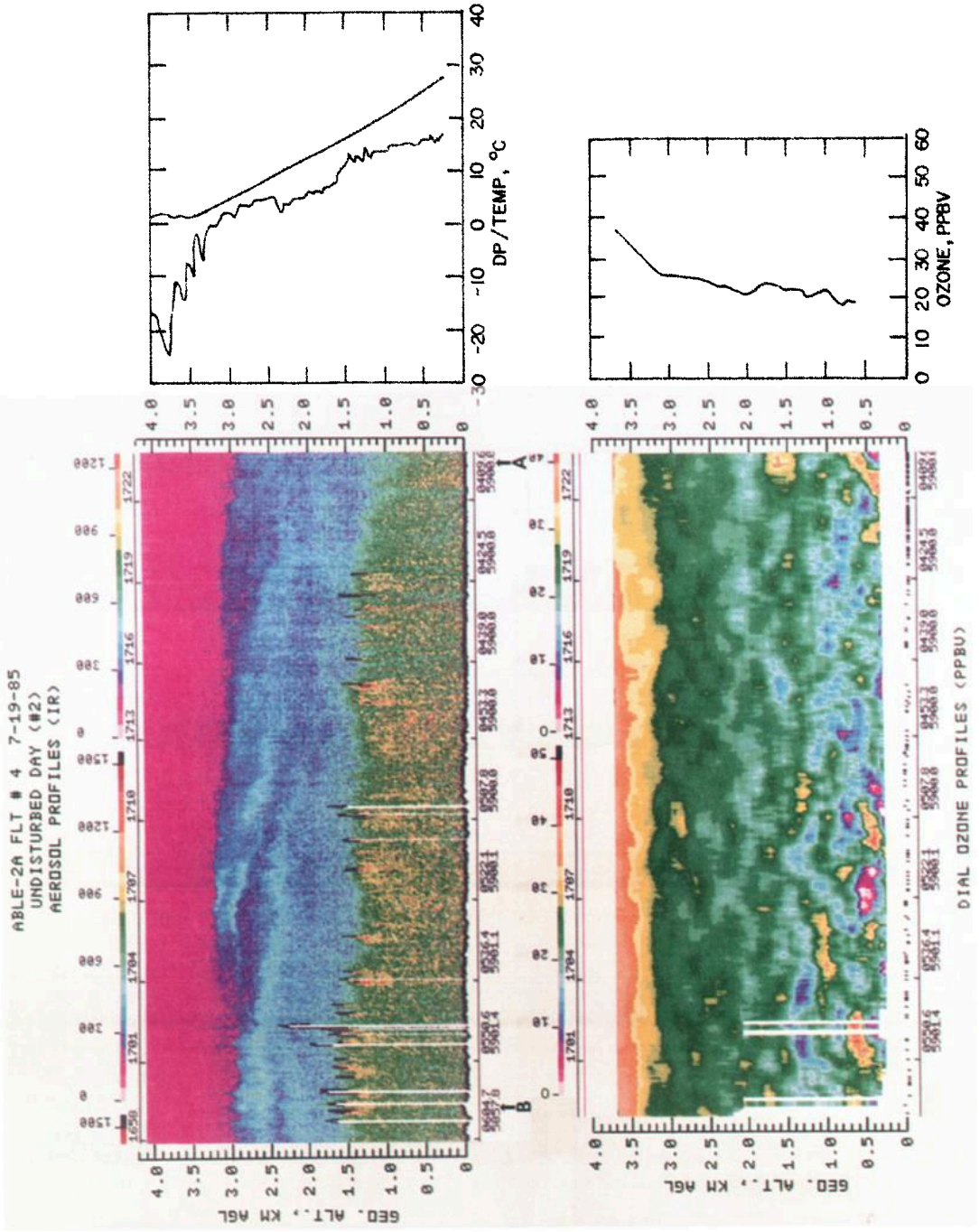

Plate 1. Aerosol and O_3 distributions obtained during undisturbed daytime conditions on July 19, 1985. Airborne lidar aerosol data (top) obtained from aircraft altitude of 4.7 km above ground level (AGL) are shown in false color display, with relative amount of atmospheric backscattering defined in color scale given at top of display. Airborne lidar O_3 data (bottom) are shown in false color display, with O_3 mixing ratio in parts per billion by volume (ppbv) defined in color scale given at top of O_3 display. In both cases, black represents values greater than maximum level given on color scale. Geometric altitudes are given in kilometers above ground level (AGL); universal time (UT) is shown at top of each display; and aircraft latitude (south) and longitude (west) at each reference time are given at bottom of display (e.g., 0604.7 over 5857.8 is 6°4.7'S latitude and 58°57.8'W longitude). Temperature and dew-point (DP) profiles from in situ measurements at point B from 1631 to 1649 UT are given beside aerosol color display. Average O_3 profile obtained from lidar data between points B and A is given beside O_3 color display.

tion [*Jacob and Wofsy*, this issue]. Nocturnal measurements over this same area (Plate 2) do not show these elevated O_3 "patches" in the 0.3 to 0.8-km region. We speculate that the O_3 "patches" in Plate 1 reflect the O_3 production processes predicted by the *Jacob and Wofsy* [this issue] model. An explanation for the irregular, relatively small-scale properties of these features can possibly be found in mechanisms of gas exchange between forest soils and the mixed layer. It is likely that gaps in the forest canopy are conduits for accelerated transport of NO from soil sources into the mixed layer. These gaps in tropical forest canopies are created by fire, high winds, and tree falls. Thus the distribution of NO in the mixed layer would be controlled, in part, by the location of gaps in the forest canopy. The variability of NO concentrations in unpolluted morning mixed layers observed by *Torres and Buchan* [this issue; also, unpublished data, 1987] add support to this hypothesis. (See additional discussions on O_3 variability in the mixed layer by *Gregory et al.* [this issue] and in the free troposphere above Manaus by Kirchhoff et al., submitted manuscript, 1987).

Plate 2 shows the O_3 and aerosol distributions found during the undisturbed nighttime case on July 25. In the aerosol color plot the nocturnal mixed layer depth can be seen to be less than 50 m, with large variability along the top of the forest canopy. The PBL has much larger aerosol loading than the previous case examined, with a high degree of spatial inhomogeneity. The temperature and dew-point plots also reflect a complex structure, with different layers having varying amounts of water vapor. The O_3 data also show considerable spatial inhomogeneity, with values from 18 ppbv in a shallow layer above the nocturnal mixed layer to 35 ppbv in a few localized regions. It should be noted that there is a general positive correlation between the regions having O_3 values in excess of 25 ppbv and the regions having enhanced aerosol loading. This is not a result of the natural downward transport of O_3 from the relatively aerosol-free regions of the free troposphere, as was the case on July 19; however, as will be discussed in more detail later, this represents a case of photochemically produced O_3 in the PBL. The average O_3 profile for the leg B-A is also shown in Plate 2. The altitude region between 1.1 and 2.4 km has an average O_3 mixing ratio in excess of 29 ppbv. This is 32% higher than the July 19 case. Since it is not possible to detect the altitude of the TWI from the data presented in Plate 2, the aerosol data from the zenith-viewing lidar channel is shown in Plate 3. The average height of the TWI was estimated to be about 3150 m acros leg B-A. The bases of several higher level stratus clouds can also be seen in the lidar data. These clouds continued to dissipate throughout the balance of the flight.

The undisturbed daytime case on July 19 was the only case during the entire experiment that did not have a region of elevated O_3 that was positively correlated with a region of aerosol enhancement. For this reason, the July 19 case was considered to be the most indicative of the background undisturbed conditions above the tropical rain forest during the dry season. To provide a better statistical basis for the average O_3 profile during the early part of the dry season, a combined average O_3 profile was calculated from two main daytime cases (July 19 and 21) and two nighttime cases (July 25 and 26), and the result is presented in Figure 2. The average profile is obtained by weighting each profile by the number of measurements used to produce it at each altitude.

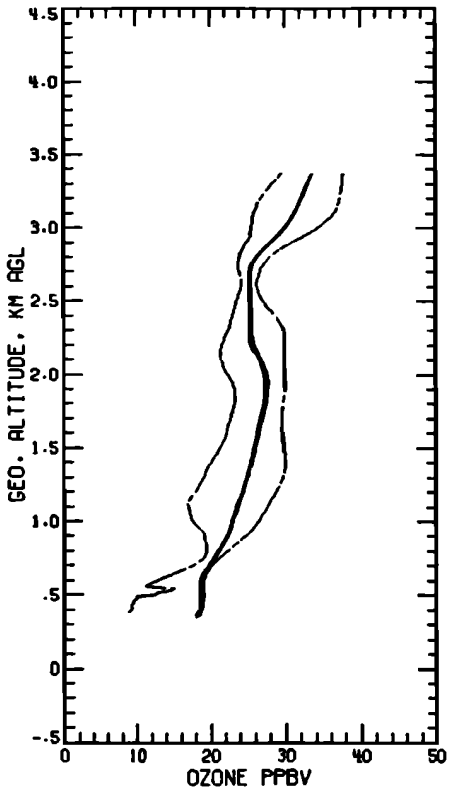

Fig. 2. Average O_3 profile from undisturbed cases on July 19, 21, 25, and 26, 1985. Envelope represents maximum and minimum O_3 mixing ratios for these cases.

The envelope represents the maximum and minimum values of the profiles at each altitude. Note that at the lowest altitude the minimum value profile resulted from a limited set of measurements between clouds on July 18 and thus was weighted considerably less than the other profiles. Compared to the O_3 profile obtained on July 19 (see Plate 1), the average O_3 profile given in Figure 2 reflects the influence of additional O_3 enhancement in the PBL due to possible photochemical activity. Table 2 presents the average atmospheric parameters and O_3 data for the undisturbed cases. In addition to the mixed layer (ML) height and TWI height, average O_3 concentrations and mixing ratios are given for the regions from about 300 m above ground level (AGL) to the top of the ML and from the top of the ML to the TWI or the maximum altitude of the DIAL data. The effective O_3 column content below the TWI to the surface is also given. This assumes that the average O_3 concentration between the TWI and ML is representative of conditions from the TWI to near the ground prior to the growth of the ML, and thus the effective O_3 column content can be used to compare cases that have different ML heights. The undisturbed daytime cases (July 18, 19, and 21) had nearly the same O_3 column content (1.58×10^{17} cm^{-2} average), even though there was a large variation in ML and TWI heights. The undisturbed nighttime cases July 25 and 26 had nearly the same O_3 column content (1.94×10^{17} cm^{-2} average); however, they were 23% above the earlier cases studied. This reflects the enhanced O_3 levels that were found in the study region after about July 21.

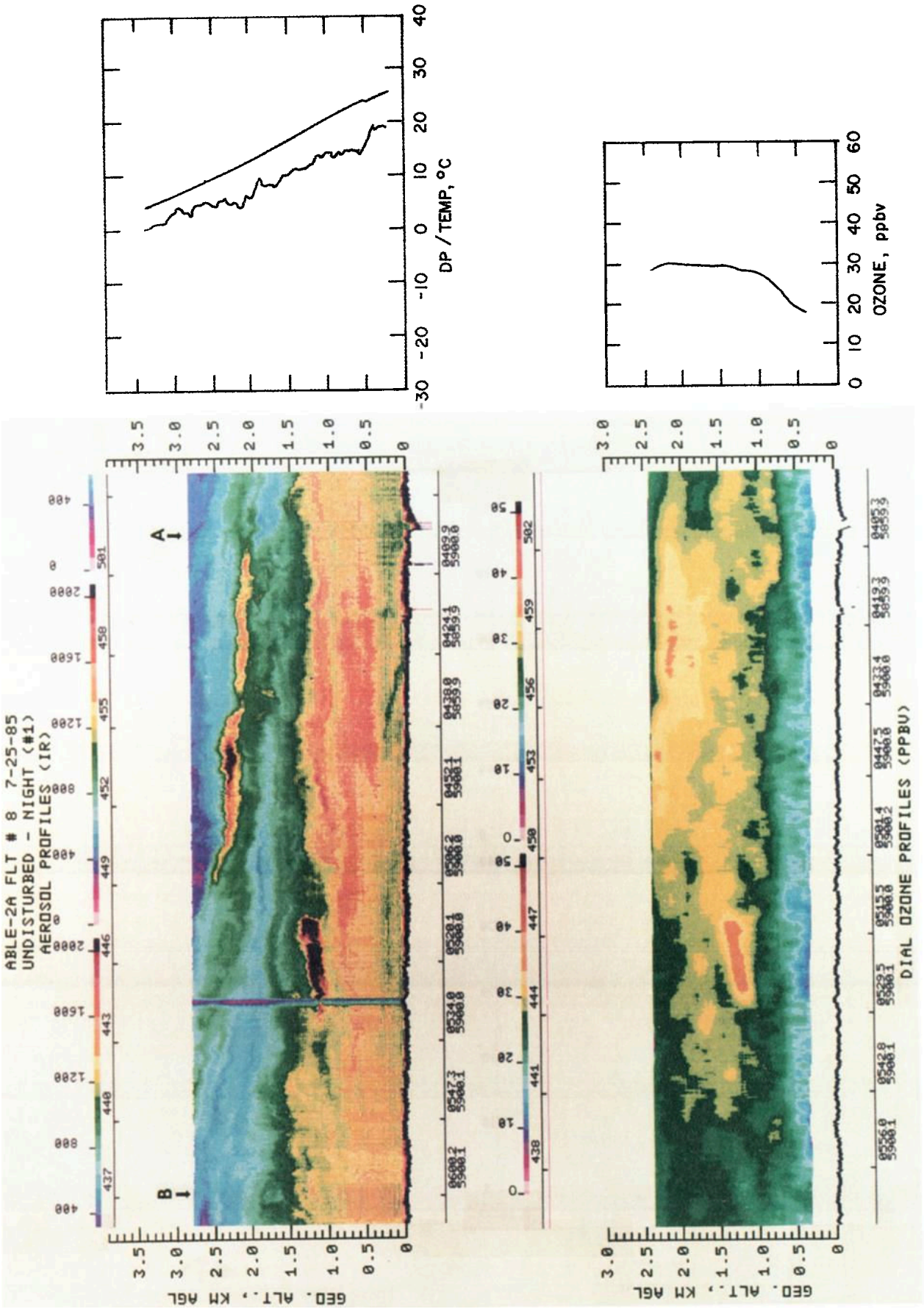

Plate 2. Aerosol and O_3 distributions obtained during undisturbed nighttime conditions on July 25, 1985. Airborne lidar measurements were made from an aircraft altitude of 3.5 km AGL.

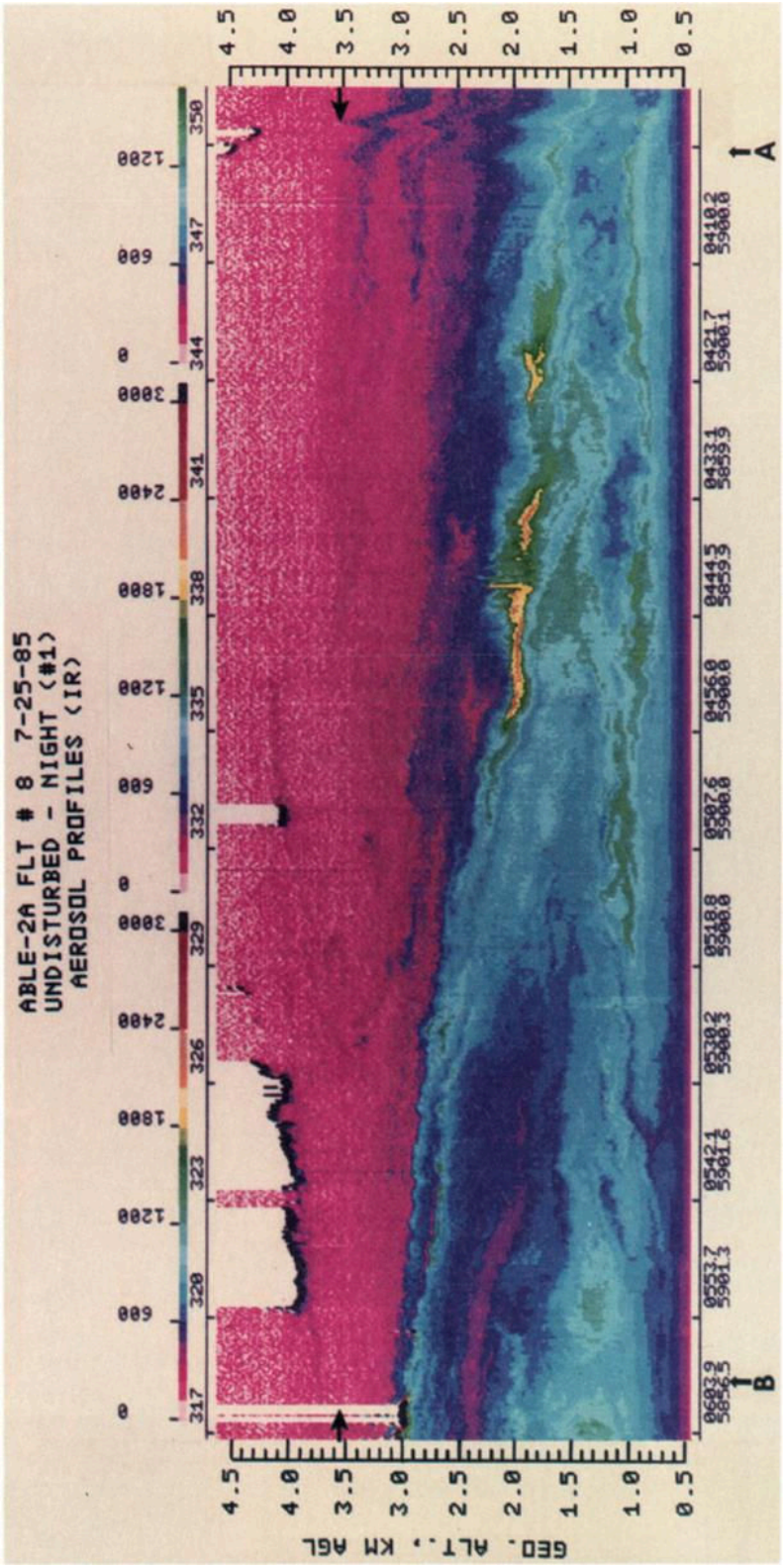

Plate 3. False color display of aerosol distribution on July 25, 1985, obtained from zenith-pointing airborne lidar aerosol channel at an aircraft altitude of 300 m AGL. Horizontal arrows indicate aircraft altitudes of "high-altitude" legs.

TABLE 2. Atmospheric Parameters and O_3 Data for Undisturbed Cases

Date (1985)	Time, UT	Location		ML Height, m	TWI Height, m	Average O_3,* (10^{11} cm^{-3})/(ppbv)		O_3 Column Content Below TWI, 10^{17} cm^{-2}
		Latitude	Longitude			Top of ML	TWI to ML Top	
July 18	1430–1503	3.0°S	57.5°W	650	3500	1.98/8.3	4.43/21.3	1.55
July 19	1659–1723	5.0°S	59.0°W	1400	3200	4.63/20.9	4.81/23.7	1.56
July 21	1541–1606	5.0°S	59.0°W	1300	3000	4.07/18.2	5.46/26.5	1.64
July 25†	0437–0502	5.0°S	59.0°W	50	3150	...	6.04/27.7	1.90
July 26†	0034–0060	6.0°S	59.0°W	50	3500	...	5.67/26.5	1.98

* Average O_3 mixing ratios calculated with standard atmosphere number density estimates at top of ML and at the midpoint between TWI and top of ML.
† Takeoff date.

Ozone and Aerosol Distributions Across Amazon Basin

Round-trip survey flights between Manaus and Belem were conducted on July 23–24, 1985, and August 8–9, 1985, to examine the spatial and temporal variations in gas and aerosol distributions from the central Amazon to the coast of Brazil. Plate 4*a* shows the aerosol and O_3 distributions obtained by the airborne DIAL system on the first portion of the flight from Manaus to Belem on July 23, 1985. The aerosol data clearly show the temporal growth of the ML depth from about 300 m at 1220 UT (0820 LST) to about 900 m at 1430 UT (1030 LST). This represents a ML growth rate of 7.7 cm s^{-1}, which compares well with values obtained during the undisturbed case studies [*Gregory et al.*, this issue; *Martin et al.*, this issue]. More aerosol layers were observed in the PBL toward the east, and these layers contained higher levels of O_3. Ozone mixing ratios exceeding 40 ppbv were found associated with the enhanced aerosol layers observed at about 1435 UT. Winds were generally from the east, at about 5 m s^{-1} from the surface to about 2.5 km AGL. Above 2.5 km AGL the wind turned with altitude to come from the southeast at 3.5 km AGL, at a speed of 6 m s^{-1}. This wind pattern is consistent with a persistent anticyclone that was centered in the vicinity of 20°–25°S and 35°–45°W, during the period July 19–31, 1985 [*Harriss et al.*, this issue]. This circulation pattern could advect gases and aerosols in the PBL from as far east as Fortaleza and Natal. Since the dry conditions had been present for a longer period of time in eastern Brazil, there was an increased chance of encountering the products of biomass burning as we made measurement toward the coast (A. Setzer, unpublished data, 1987). The positive correlation between aerosols, O_3, and carbon monoxide (CO) [*Andreae et al.*, this issue] in some of the PBL layers indicates that their source was from biomass burning at an upwind location. Since O_3 is not directly released in the burning process, it results from photochemical production in the air mass as it is advected over several days in the PBL or free troposphere.

An initial line of clouds associated with a sea breeze front was observed about 15 km east of the point J′, shown in Plate 4*a* (300 km southwest of the coast) on July 23. Plate 4*b* shows the aerosol and O_3 distributions in the PBL to the east of the front, which were more comparable to the background levels found near Manaus in the first few weeks of the dry season. The coast of Brazil was crossed at about 1701 UT, and the change in aerosol characteristics from the ML over the forest (near point M) to the marine ML (near point R) can be seen in the lidar aerosol data. The sea-salt aerosols in the marine ML were found to produce greater than 3 times more backscattering at 1064 nm than did the aerosols observed over the forest. The lidar return at this wavelength is most sensitive to aerosols with diameters larger than 0.5 μm, and in situ measurements of aerosols with diameters greater than 0.5 μm showed an increase in number density from 0.25 cm^{-3} over the forest between point J′ (see Plate 4*a*) and point M (see Plate 4*b*) at 150 m AGL to 1.47 cm^{-3} in the marine ML at 150 m ASL. There were no substantial differences in the measured size distributions for the two cases. The approximate percentage of aerosols in each diameter range was 75% in the 0.5 to 1.0-μm range, 18% in the 1.0 to 1.5-μm range, 6% in the 1.5 to 2.0-μm range, and 1% in the 2.0 to 2.5-μm range. The magnitude of the lidar backscatter return also depends on the aerosol shape, refractive index, and size distribution and on the concentration for aerosols with diameters less than 0.5 μm.

Figure 3 shows the average O_3 profiles obtained from the DIAL measurements along the legs identified in Plates 4*a* and 4*b*. The O_3 mixing ratios were found to increase at all altitudes toward the sea breeze front. At an altitude of 1.5 km AGL, the O_3 mixing ratio increased 75% over a distance of 490 km. The average O_3 profile over leg MN, east of the sea breeze front, is similar to the average O_3 profile shown in Figure 2 for the undisturbed cases near Manaus in July, and the average profile over leg QR represents a typical O_3 distribution in the marine environment. The wind over the water was from the east at all altitudes up to 3.0 km ASL, and it is assumed that the air mass encountered along this leg was background air from the western Atlantic.

The O_3 distribution for July 1985 between Manaus and Belem is shown in Figure 4. All average O_3 profiles from undisturbed case studies and the round-trip survey flight between Manaus and Belem were used to produce the isopleth distribution. Multiple measurements made within 0.5° longitude were averaged together, and a vertical smoothing of 300 m was applied to each average profile prior to constructing the isopleths. See Tables 2 and 3 for the locations of the average O_3 profiles on July 19, 21, 23, 24, 25, and 26. Note that the average profile from July 18 was not used because of the large amount of cloud cover encountered during the mission. Figure 4 shows the earliest available average cross-sectional distribution of O_3 between Manaus and Belem in the dry season. There appears to be little variation in the average O_3 distribution between 59°–56°W. This represents the average background undisturbed O_3 distribution over the forest near Manaus. The region of O_3 enhancement between 1.0–2.5 km AGL and 56°–51°W is generally confined to the PBL region between the ML top and the TWI. Regions containing O_3 mixing ratios exceeding 30 ppbv are generally found above the TWI

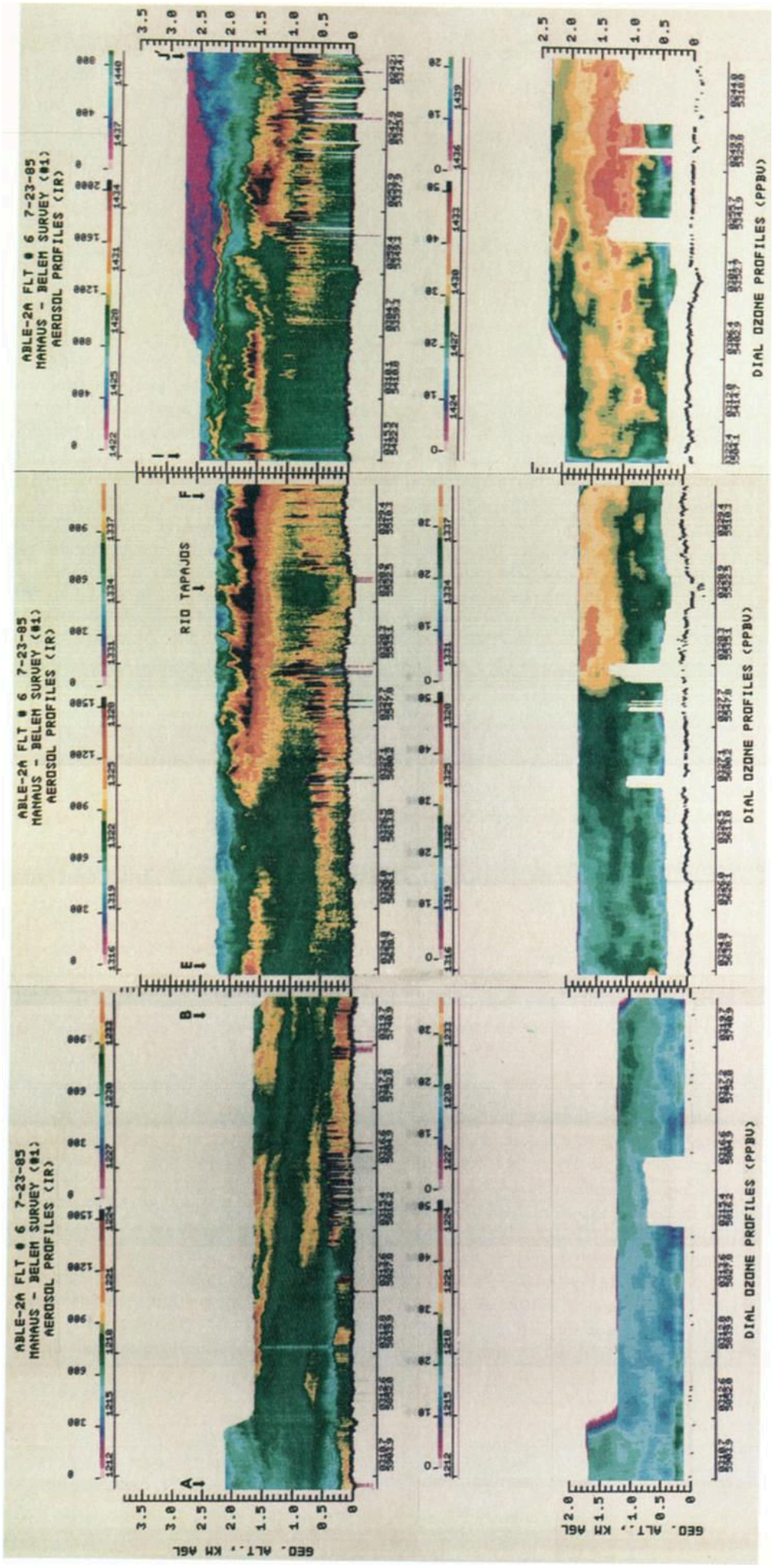

Plate 4a. Aerosol and O_3 distributions obtained on Manaus to Belem survey flight on July 23, 1985. Entire plot spans distance from about 60 to 720 km east of Manaus. Note change in aerosol relative backscattering scale for leg IJ'.

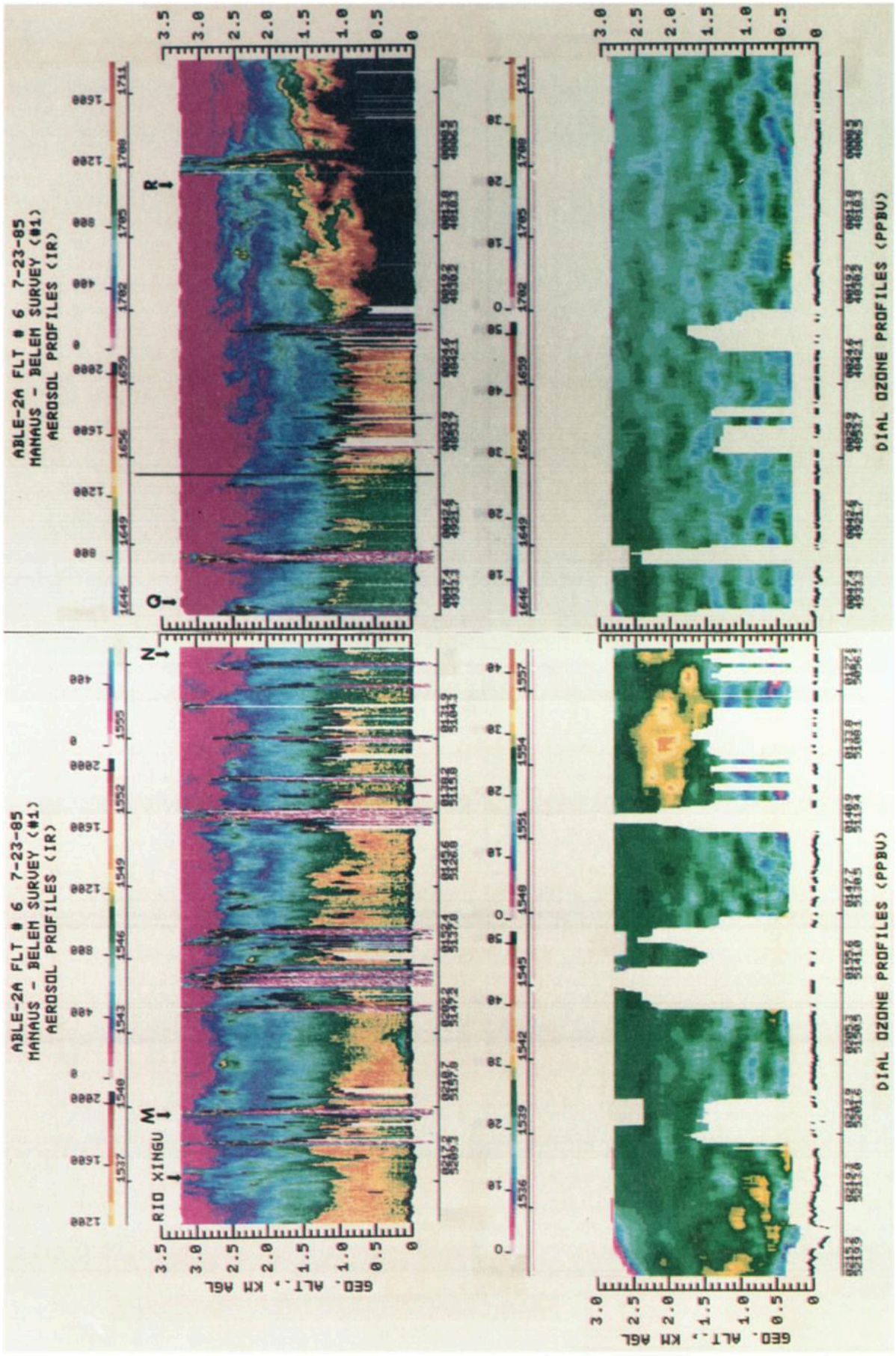

Plate 4b. Continuation of data presented in Plate 4a for Manaus to Belem survey flight on July 23, 1985. Coast of Brazil (about 1200 km east of Manaus) crossed at 1701 UT. Note that aerosol relative backscattering scales are the same as used for leg II' in Plate 4a.

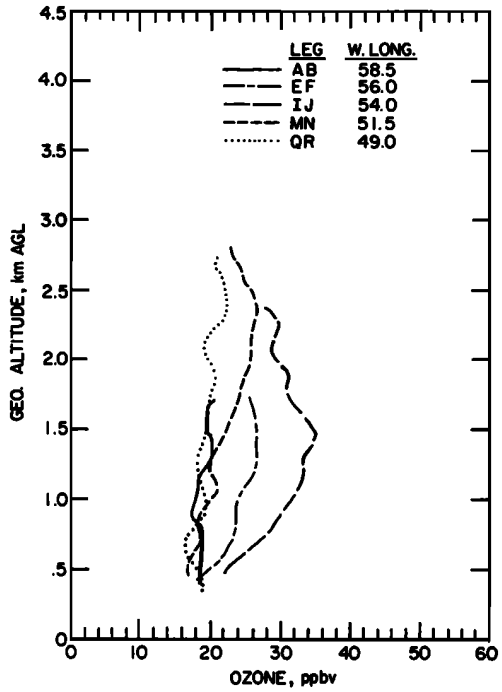

Fig. 3. Average O_3 mixing ratio profiles obtained from airborne DIAL data on July 23, 1985. Average O_3 profiles correspond to data legs shown in Plates 4*a* and 4*b* and approximate west longitude of the midpoint of each leg is also given.

level (about 3.2 km AGL) in the background O_3 distributions near Manaus. The transition to the average marine background O_3 distribution can be seen east of 51°W. The average vertical gradient of O_3 between 1–3 km AGL over the forest between Manaus and Belem was 3.3 ppbv km^{-1}. This value is comparable to the average value of 2.8 ppbv km^{-1} found under undisturbed conditions near Manaus.

A second round-trip survey flight between Manaus and Belem was conducted on August 8–9, 1985, which was 16 days after the first round-trip flight. Plate 5*a* shows the aerosol and O_3 data for the initial part of the flight from Manaus to Belem. Strong aerosol layers were observed in the lidar data between 1321–1339 UT in the region above 1.8 km AGL. These layers were highly attenuating for the 1064-nm lidar pulse, and this resulted in the loss of visibility for the atmospheric features below the aerosol layers. These layers can be seen along leg EF to be as low as 1.2 km AGL. The scale for display of the aerosol backscattering data was changed to show the magnitude of the backscattering across the layers. Ozone mixing ratios exceeding 50 ppbv were measured across these aerosol-enriched layers. The DIAL O_3 data was limited in altitude in some regions as a result of signal attenuation across the aerosol layers and clouds. Where O_3 data between 0.4–1.0 km AGL could be obtained, the O_3 values were generally enhanced over July background levels. These layers were found to result from the transport of biomass-burning plumes from a region about 500 km to the southeast of the aircraft flight track [*Andreae et al.*, this issue]. The elevated O_3 levels are interpreted as evidence of the photochemical production of O_3 in the plumes during transport from the source region. Plate 5*b* shows the aerosol and O_3 data on the remainder of the flight to Belem. While the amount of aerosol loading in the layers observed along leg GH appears to be reduced from those to the west, there is substantial O_3 enhancement (>45 ppbv) associated with the layers. There did not appear to be a strong sea breeze front present on August 8; however, as we approached the coast along leg IJ, there was no evidence of distinct layers in the PBL in the aerosol or O_3 data. Above the marine ML, which had an average depth of about 700 m near point J, the regions having enhanced O_3 levels had low aerosol backscattering. This negative correlation between aerosols and O_3 is strongly indicative of air found in the upper troposphere. Also, CO concentrations [*Sachse et al.*, this issue] were negatively correlated with O_3 in this same region. This is further evidence that the enhanced O_3 detected along leg IJ was not related to biomass burning.

An isopleth plot of the average O_3 data obtained on August 8 and 9, 1985, is shown in Figure 5. In addition to the DIAL data, in situ O_3 profiles at 57.9° and 60°W were included in this analysis. This average cross section shows an increased level of O_3 across the entire region compared to the July data set (see Figure 4). In both data sets there is a common trend toward lower O_3 levels near the coast. The average vertical O_3 gradient in the 1- to 3-km altitude range increased to 5.0 ppbv km^{-1} over the forest during this period, and this reflects an increase in the photochemical production of O_3 near the top of the PBL. The O_3 production was greater to the west of Belem, as is indicated by the 35-ppbv O_3 isopleth, which slopes downward from 3.2 km AGL near the coast to 1.3 km AGL east of Manaus. In addition, the average O_3 levels greatly exceed 40 ppbv within the PBL over extensive areas in August where comparable areas only slightly exceeded 30 ppbv in July.

To quantify the change in O_3 levels in the PBL between July and August, the effective O_3 column density below the TWI was calculated along each leg of the survey flights by assuming that the average O_3 concentration determined between the top of the ML and the TWI was indicative of the entire PBL. This permits the comparison of O_3 data from different survey flights without the influence of a diurnally varying ML depth. Table 3 presents the values of average O_3 concentrations and mixing ratios in the PBL and the O_3 column contents for each leg of the survey flights. Data are only given for cases where greater than 50% of the PBL above the ML was sampled. Figure 6 presents a comparison of the average O_3 column densities determined for the July 23–24 and August 8–9 round-trip survey flights between Manaus and Belem. Data obtained at the same geographical location (within 0.5°) on outbound and return survey flights were averaged for each time period. The average O_3 column density for July 23–24 is relatively constant over the forest with an average value of 1.48×10^{17} cm^{-2} (within 6% of average value found for July 18, 19, and 21 near Manaus). Near the coast there is a trend to lower amounts of O_3 below the TWI with a value of 1.19×10^{17} cm^{-2} over the water. The data from August 8–9 show a dramatic O_3 increase in the PBL. The area near Manaus has only a moderate increase in O_3 (35%) compared to the 100% increase near 56°W. There is again a decrease in O_3 column density toward the coast; however, in this region, the August values are still about 60% higher than in July. The total O_3 increase in the PBL along the cross section from 60°–48°W longitude over the 16-day period between round-trip survey flights was 59%. The average height of the TWI also increased over this region from 2661 to 3510 m over the same period. Since the average O_3 gradient above the TWI on July 23–24 was about

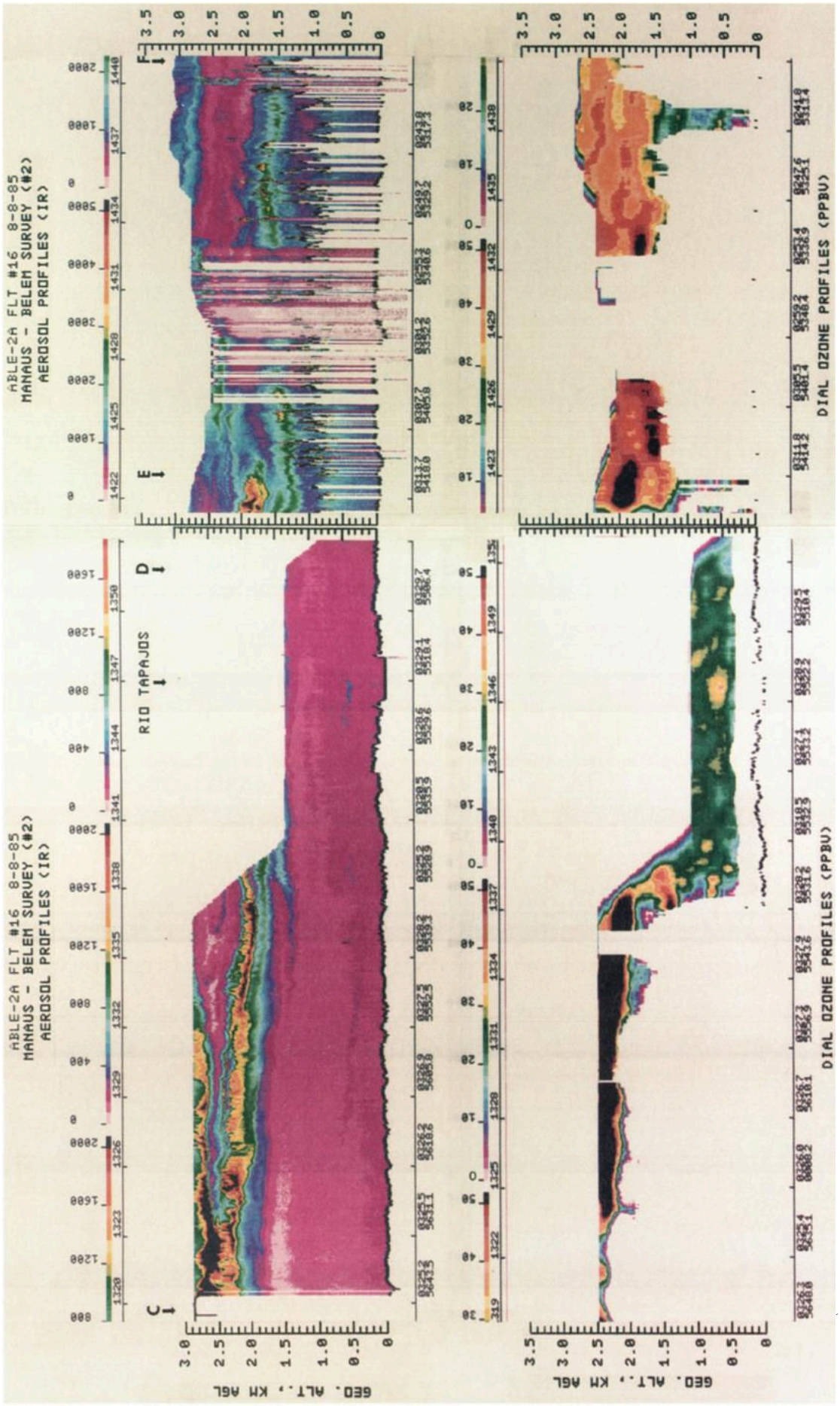

Plate 5a. Aerosol and O_3 distributions obtained on Manaus to Belem survey flight on August 8, 1985. Legs CD and EF correspond closely to legs EF and IJ', respectively, in Plate 4a. Note differences in aerosol relative backscattering scales for legs CD and EF.

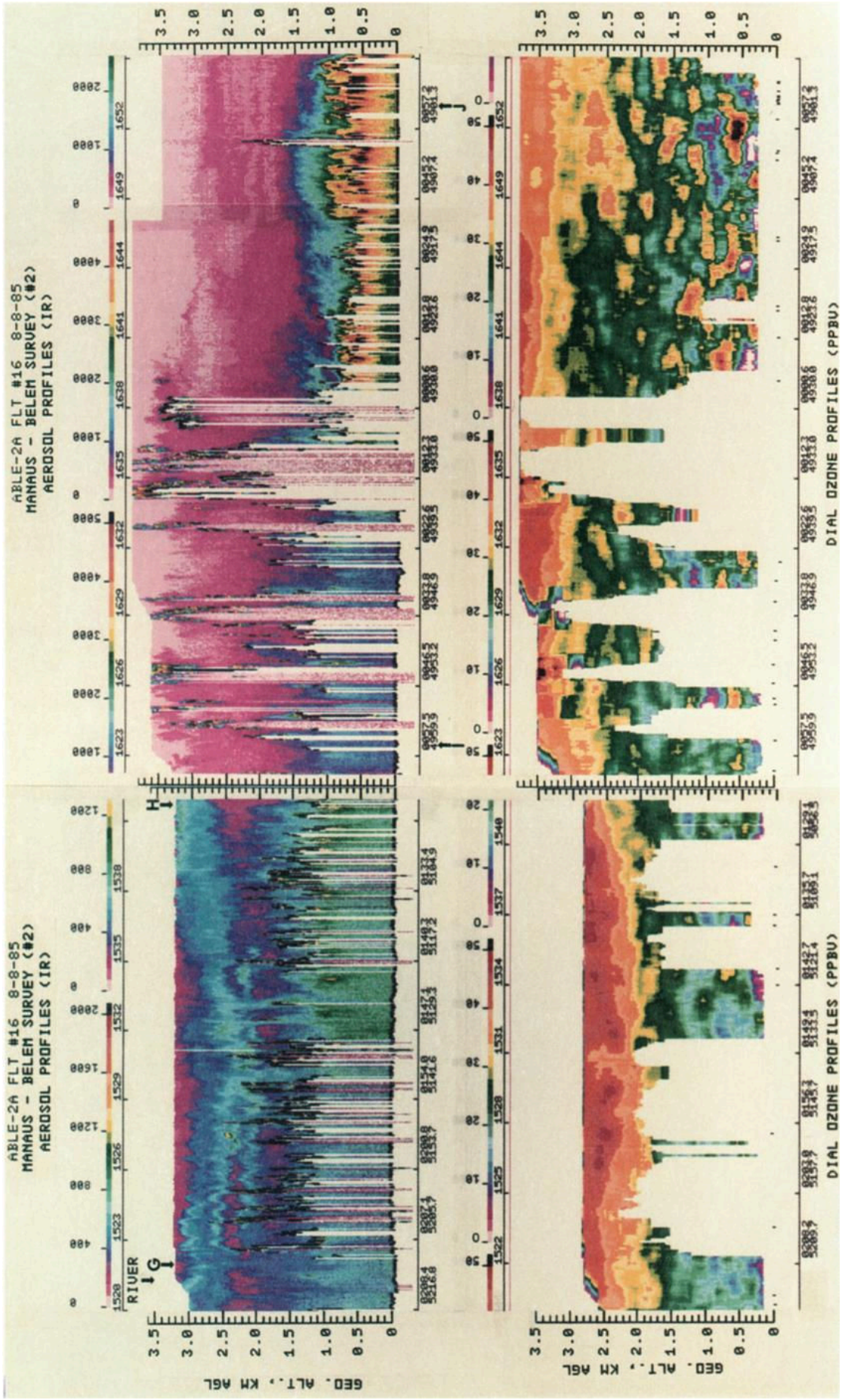

Plate 5b. Continuation of data presented in Plate 5a for Manaus to Belem survey flight on August 8, 1985. Legs GH and IJ correspond closely to legs MN and QR, respectively, in Plate 4b. Note differences in the aerosol backscattering scales for legs GH and IJ.

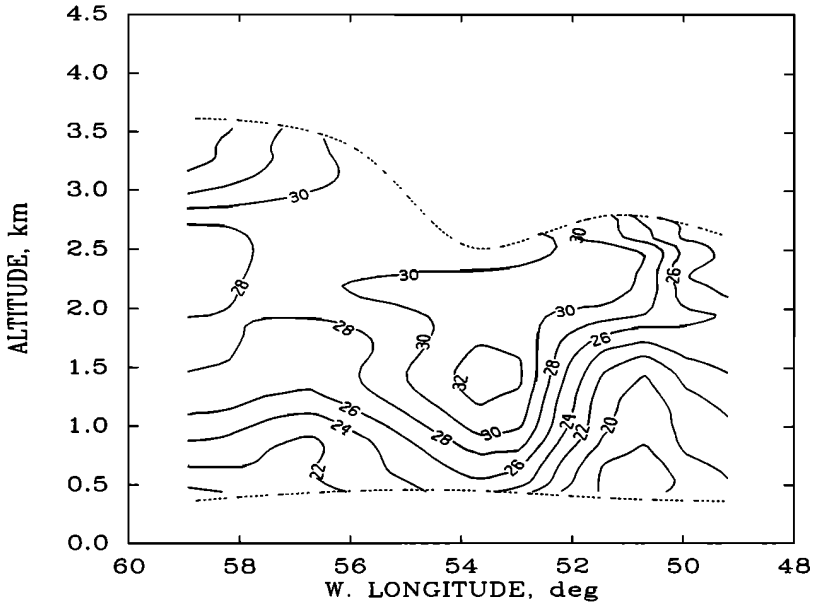

Fig. 4. Isopleths of O_3 mixing ratios (ppbv) between Manaus and Belem for July 1985 generated from average O_3 profiles for undisturbed cases near Manaus (July 18, 19, 21, 25, and 26) and from round-trip survey flight on July 23 and 24. The dashed lines represent the vertical extent of the O_3 data.

4.2 ppbv km^{-1}, the extra amount of O_3 possibly transported into the PBL as a result of the increase in height of the TWI would represent only a 2.2% increase in the O_3 column content. This indicates that most of the increase in O_3 is locally produced in the PBL as a result of photochemical activity.

A survey flight on August 5, 1985, to the west of Manaus provided information on the distribution of aerosols and O_3 along the Rio Solimões to Tabatinga, which is on the border of Columbia. Plate 6*a* presents airborne DIAL data that show a considerable amount of O_3 in the old PBL above a growing ML on the morning of August 5. Layers having enhanced aerosol scattering were noted along the flight track (see legs DE and FG). With the exception of the aerosol layers associated with clouds near 1223 UT, the other aerosol layers had O_3 levels exceeding 40 ppbv and enhanced CO concentrations [*Sachse et al.*, this issue]. This indicates that the increased O_3 concentrations were caused by photochemical production in association with biomass burning. In addition, numerous fires were noted during this flight in the vicinity of the Rio Solimões. The return flight from Tabatinga to Manaus was generally upwind of the river at a constant altitude. An example of the aerosol and O_3 data for this flight is shown in Plate 6*b*. Except for a localized plume of aerosols and O_3 encountered between 1925–1934 UT, which appeared to have an associated residual layer

TABLE 3. Atmospheric Parameters and O_3 Data for Survey Missions Between Manaus and Belem

Date (1985)	Time, UT	Location		ML Height, m	TWI Height, m	Average O_3,* $(10^{11}$ cm$^{-3})$/(ppbv)		O_3, Column Content below TWI,† 10^{17}/cm^{-2}
		Latitude	Longitude			Top of ML	TWI to ML Top†	
July 23	1211–1234	3.0°S	58.5°W	300	2750	...	...	...
	1316–1339	3.5°S	56.0°W	600	2800	4.78/19.9	5.63/26.1	1.58
	1422–1442	3.0°S	54.0°W	900	3000	6.00/25.8	6.80/31.5	2.04
	1539–1558	2.0°S	51.5°W	1100	2700	4.38/19.1	4.96/23.5	1.34
	1646–1707	0.5°S	49.0°W	1100	2650	4.31/18.8	4.20/19.8	1.11
July 24	1319–1348	0.0°S	49.5°W	800	2400	4.89/20.7	5.31/24.4	1.27
	1440–1458	2.0°S	51.5°W	950	2600	3.68/15.9	5.55/25.8	1.44
	1550–1608	3.0°S	53.5°W	1100	2400	4.76/20.8	5.94/27.6	1.43
	1701–1719	3.5°S	56.0°W	1400	2650	4.72/21.3	5.68/27.2	1.51
August 8	1320–1352	3.5°S	55.5°W	600	3850	5.12/21.3	8.01/39.1	3.08
	1423–1442	3.0°S	53.8°W	1000	3900	3.96/17.1	7.49/37.4	2.92
	1522–1542	1.8°S	51.5°W	1300	3650	4.51/20.1	6.57/32.8	2.40
	1623–1653	0.0°S	49.5°W	1200	3600	5.42/23.9	5.56/27.7	2.00
August 9	1349–1409	0.0°S	49.5°W	1000	3200	5.44/23.6	6.23/30.1	1.99
	1451–1510	1.8°S	51.5°W	900	3100	4.36/18.7	6.34/30.3	1.97
	1547–1605	3.0°S	53.8°W	900	3000	3.34/14.3	6.74/32.1	2.02
	1635–1659	3.5°S	55.5°W	1400	3600	6.28/28.3	...	...
	1659–1719	3.2°S	57.0°W	1400	3690	6.07/27.3	8.94/45.2	3.30

* Average O_3, mixing ratios calculated with standard atmosphere number density estimates at top of ML and at the midpoint between TWI and top of ML.

† O_3 data not shown where less than 50% of region between TWI and ML was sampled.

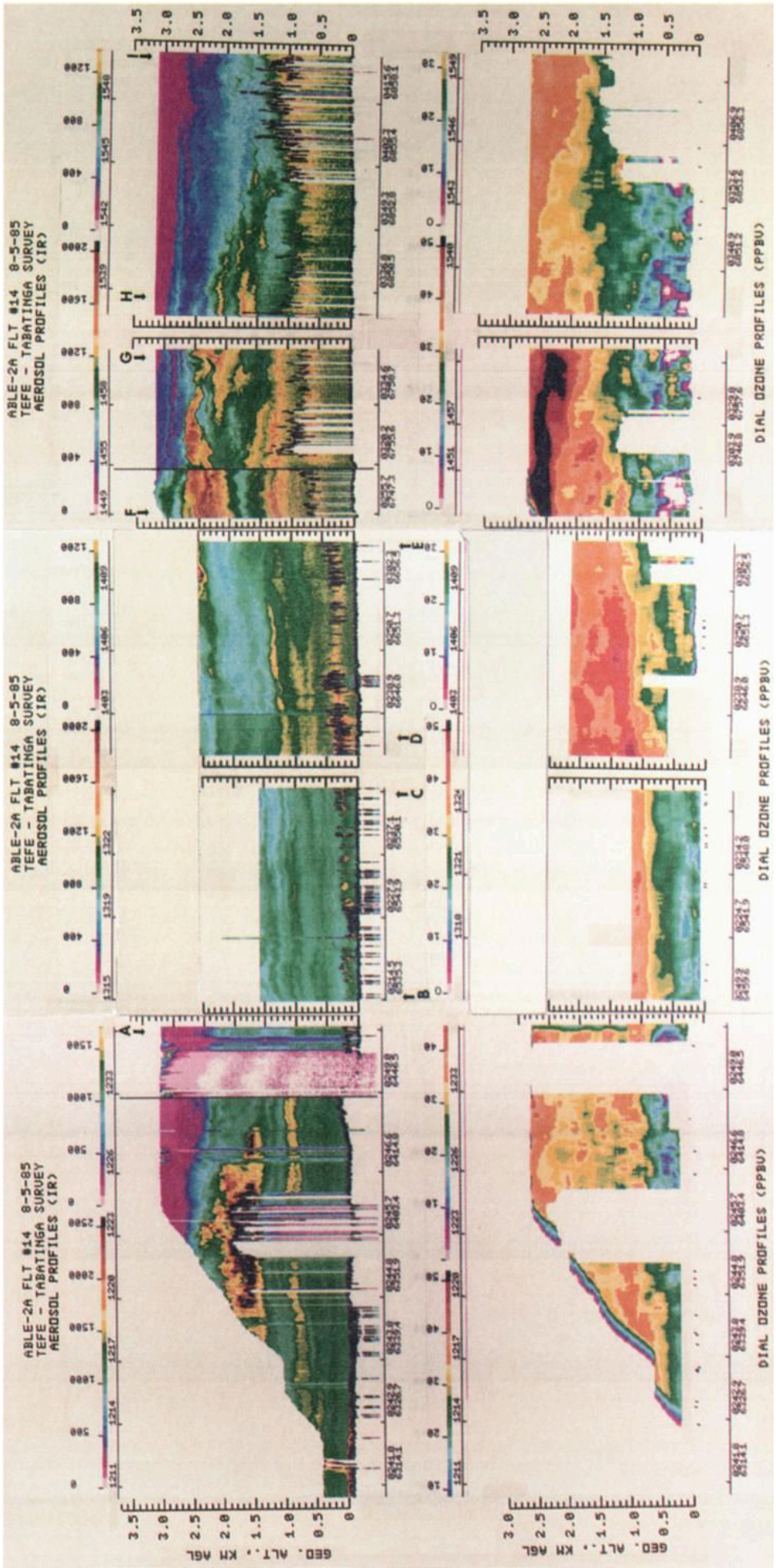

Plate 6a. Aerosol and O_3 distributions obtained on Tefe to Tabatinga survey flight on August 5, 1985. Flight was along the Rio Solimões. Note change in aerosol relative backscattering scale used for data after 1315 UT.

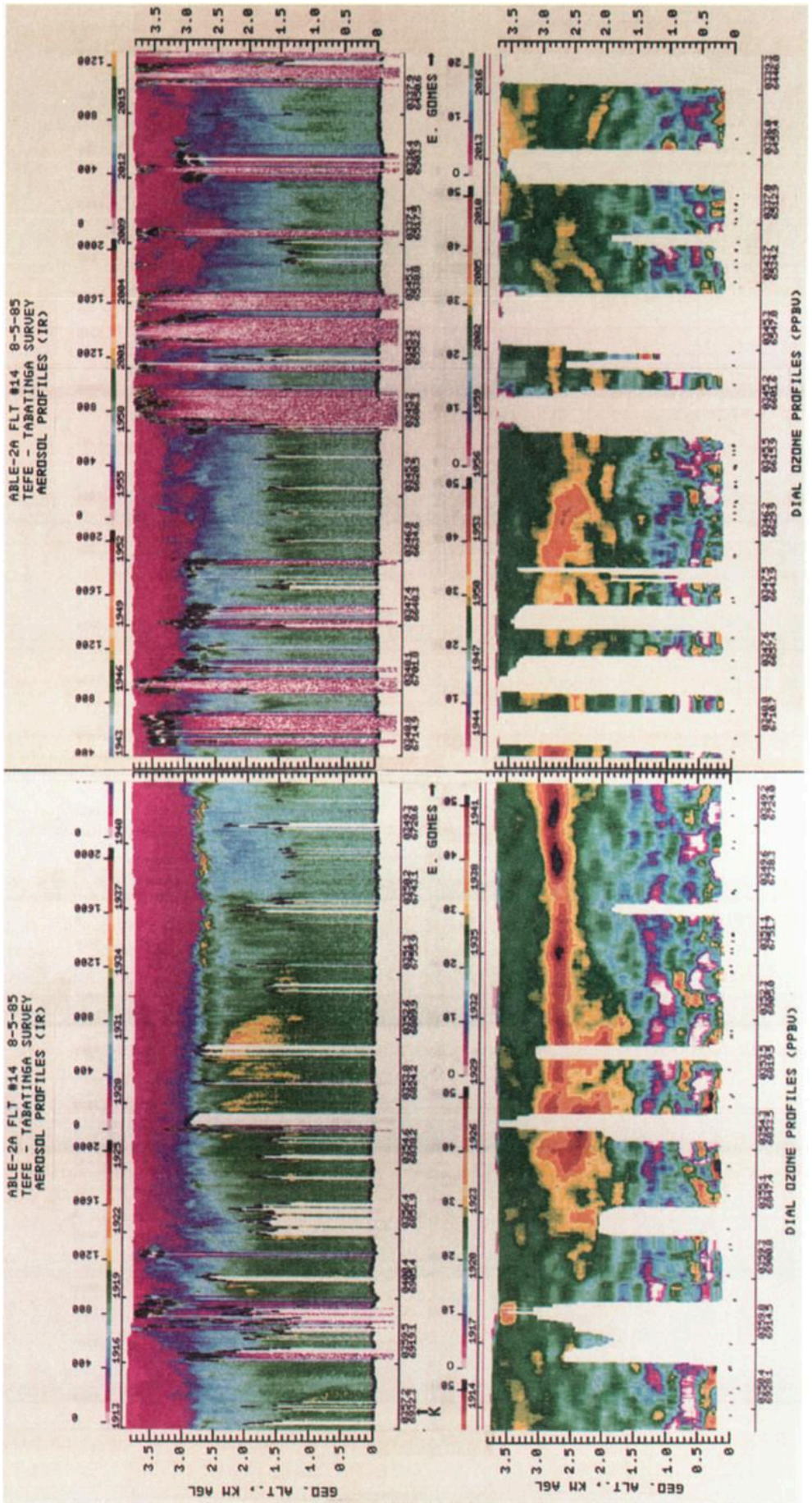

Plate 6b. Aerosol and O_3 distributions obtained on constant-altitude return flight from Tabatinga toward Manaus. Flight was southeast of the Rio Solimões by about 0.5°.

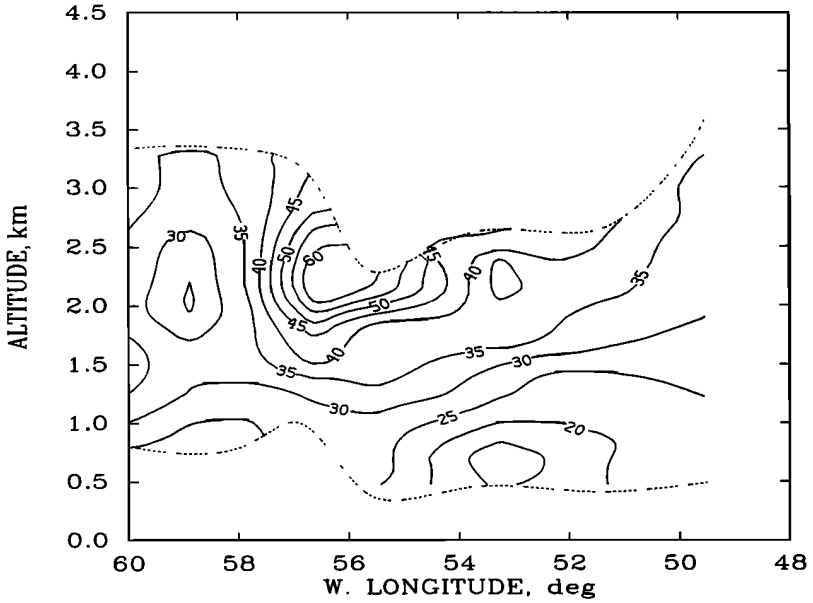

Fig. 5. Isopleths of O_3 mixing ratios (ppbv) between Manaus and Belem on August 8–9, 1985, generated from in situ O_3 profile data obtained near Manaus and average lidar O_3 profiles obtained on round-trip survey flight.

trapped beneath the TWI, the average aerosol and O_3 levels along this atmospheric cross section were lower than those found along the river. Table 4 presents the average O_3 values in the PBL for this flight and the survey flight between Manaus and Tefe on August 6. A plot of the average O_3 concentrations below the TWI for these two flights is given in Figure 7. The PBL O_3 concentration in the outbound leg along the Rio Solimões on August 5 was found to be about 38% higher than the O_3 concentration on the return leg, which was upwind of the river. This increase over a distance of typically less than 100 km suggests a localized production of O_3 in conjunction with biomass burning. The data obtained between Manaus and Tefe on August 6 were obtained over the same locations on outbound and return portions of the flight. The average O_3 concentrations showed good agreement over the entire flight (see Table 4 and Figure 7), and the average level of O_3 in the PBL was found to be comparable to the undisturbed July levels near Manaus,

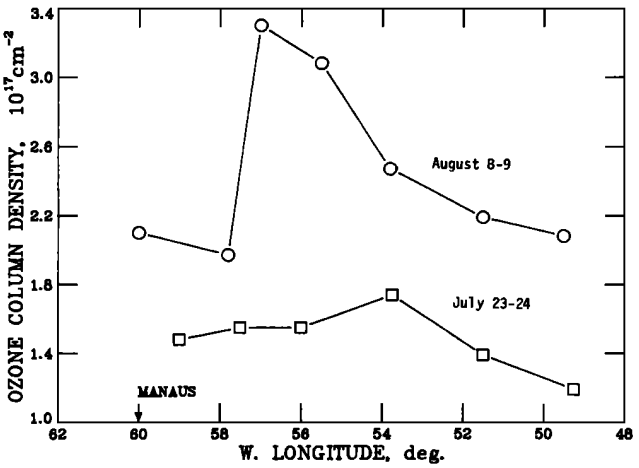

Fig. 6. Ozone column densities below trade wind inversion.

which indicates that the effects of biomass burning were not as evident over that portion of the Rio Solimões.

To obtain the distribution of O_3 across the entire Amazon Basin, a composite of the O_3 profile measurements was produced from data from all of the flights between August 5–9, 1985. Ozone profiles were averaged together when more than one measurement was made within a 0.5° longitude interval. Figures 8 and 9 show the resulting distribution of O_3 across the Amazon Basin in early August 1985. The elevated concentrations of O_3 in the PBL to the east of Manaus as a result of local and upwind biomass burning is in contrast to the low levels to the west of Manaus. The area west of Manaus was subject to a longer wet season than to the east of Manaus, and the synoptic weather patterns were not favorable for long-range transport of biomass-burning products to this region from the dry savannah regions to the southeast. Only in the river basin to the east of Tabatinga was there evidence of enhanced O_3 levels as a result of local biomass burning, and these areas were in the upper PBL (>2 km AGL), as was the case east of Manaus. It should be noted that the height of the TWI, as determined from lidar and in situ measurements on the Electra, did not have a major variation across the Basin during August. The average TWI height increased by less than 10% from 3.1 km AGL to the west of Manaus to 3.4 km AGL to the east of Manaus, with no other apparent large-scale trend.

GLOBAL IMPLICATIONS

Geochemical mass balance calculations [*Seiler and Crutzen*, 1980; *Crutzen et al.*, 1979] and preliminary observations from aircraft and satellites [*Delany et al.*, 1985; *Fishman et al.*, 1986] have led to the hypothesis that tropical biomass burning could be a significant source of gases which enhance global photochemical O_3 production. The ABLE 2A remotely sensed O_3 and aerosol distributions reported in this paper and by *Andreae et al.* [this issue] confirm that biomass burning under dry-season meteorological conditions produces synoptic-scale O_3 enhancements in the PBL over

TABLE 4. Atmospheric Parameters and O_3 Data for Survey Missions West of Manaus

Date (1985)	Time, UT	Location		ML Height, m	TWI Height, m	Average O_3,* $(10^{11}$ cm$^{-3})$/(ppbv)		O_3 Column Content below TWI,† 10^{17}/cm^{-2}
		Latitude	Longitude			Top of ML	TWI to ML Top†	
August 5	1211–1236	2.8°S	64.0°W	400	3400	6.42/26.2	6.62/31.4	2.25
	1315–1325	2.5°S	65.8°W	300	3100	4.51/18.3	...	...
	1402–1411	2.8°S	66.8°W	400	3200	4.30/17.6	7.72/36.1	2.47
	1449–1500	3.5°S	68.0°W	800	3200	3.55/15.0	7.51/35.9	2.40
	1539–1550	4.0°S	69.0°W	1000	2900	3.56/15.4	6.25/29.8	1.81
	1914–1926	4.0°S	69.0°W	1400	2900	3.47/15.6	4.98/23.7	1.44
	1927–1938	3.8°S	68.0°W	1400	2900	3.42/15.4	5.98/29.0	1.73
	1938–1950	3.8°S	67.0°W	1400	3100	3.42/15.4	5.35/26.2	1.66
	1950–2002	3.8°S	66.2°W	1400	2900	3.61/16.3	5.52/26.8	1.60
	2002–2014	3.8°S	65.2°W	1400	3000	3.65/16.4	4.87/23.8	1.46
	2014–2026	3.8°S	64.5°W	1400	2900	3.49/15.7	4.42/21.5	1.28
	2026–2038	3.5°S	63.5°W	1400	3000	4.06/18.3	4.58/22.3	1.37
	2038–2052	3.5°S	62.5°W	1400	3000	4.01/18.1	5.23/25.5	1.57
August 6	1209–1219	3.8°S	61.2°W	200	3450	...	5.85/27.3	2.02
	1305–1316	4.0°S	62.2°W	300	3350	3.81/15.4	5.80/27.1	1.94
	1400–1410	4.0°S	63.2°W	500	3450	5.01/20.6	5.70/27.1	1.97
	1450–1504	3.0°S	64.2°W	700	2900	3.30/13.9	5.49/25.6	1.59
	1546–1557	2.5°S	65.5°W	750	2900	3.19/13.5	5.49/25.6	1.59
	1640–1651	3.0°S	64.2°W	1150	3690	4.31/18.9	5.20/25.9	1.92
	1651–1703	3.8°S	63.8°W	1150	3690	4.93/21.6	5.76/28.7	2.13
	1704–1716	4.0°S	63.0°W	1100	3400	4.59/20.0	5.97/29.3	2.03
	1716–1728	3.8°S	62.2°W	1300	2800	4.36/19.5	6.01/28.9	1.68
	1728–1739	3.5°S	61.5°W	1300	2900	5.35/23.9	5.39/26.0	1.56

* Average O_3 mixing ratios calculated with standard atmosphere number density estimates at top of ML and at the midpoint between TWI and top of ML.

† O_3 data not shown where less than 50% of region between TWI and ML was sampled.

remote, undisturbed regions of the central Amazon Basin. The large-scale upper atmospheric subsidence which produces the dry-season climate also leads to an accumulation of pollutants of both local and regional origin in the central Amazon PBL. The ABLE 2A data show an increase in PBL O_3 of approximately 3–4% per day over the eastern half of the Amazon Basin during the early to middle phases of the dry season. The late dry-season data of *Crutzen et al.* [1985] indicate that concentrations of O_3 and CO continue to increase throughout the dry season. The increase in convective activity associated with the early stages of the wet season, which generally begins in September and October, could transport the accumulated O_3, CO, and other relatively insoluble gases to upper tropospheric altitudes [*Dickerson et al.*, 1987; *Garstang et al.*, this issue], producing the large-scale enhancements observed from space shuttle and satellite measurements [*Fishman et al.*, 1986; *Reichle et al.*, 1986].

The O_3 distributions reported in this paper also show preliminary evidence for natural photochemical O_3 production in the undisturbed, unpolluted mixed layer over the rain forest. These data support the model calculations of *Jacob and Wofsy* [this issue] for the ABLE 2A conditions and the speculation that photochemical O_3 production may occur on a global scale in the mixed layer over rain forests. The widespread pollution of the Amazon PBL during the dry season limits direct observations of natural photochemical O_3 production; these processes should be more readily observed during undisturbed periods of the wet season.

Future considerations of the global O_3 budget will require further quantification of both natural and anthropogenic sources of O_3 in the tropics. The spatial and temporal

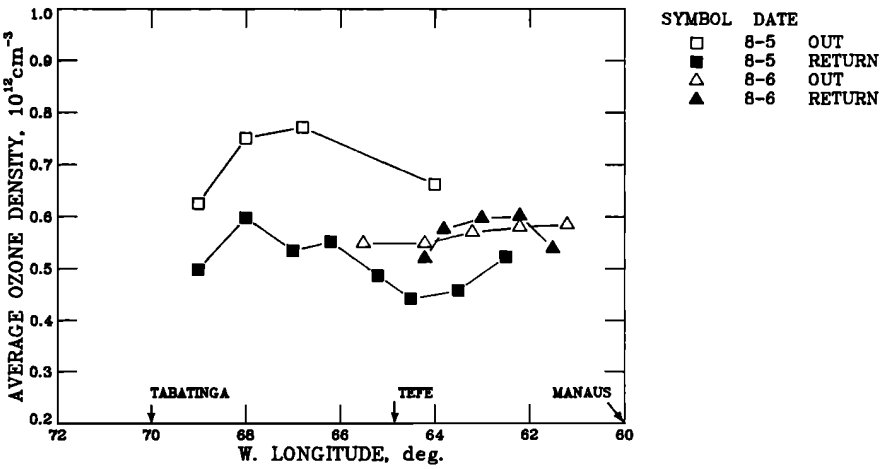

Fig. 7. Average O_3 concentrations between top of mixed layer and trade wind inversion.

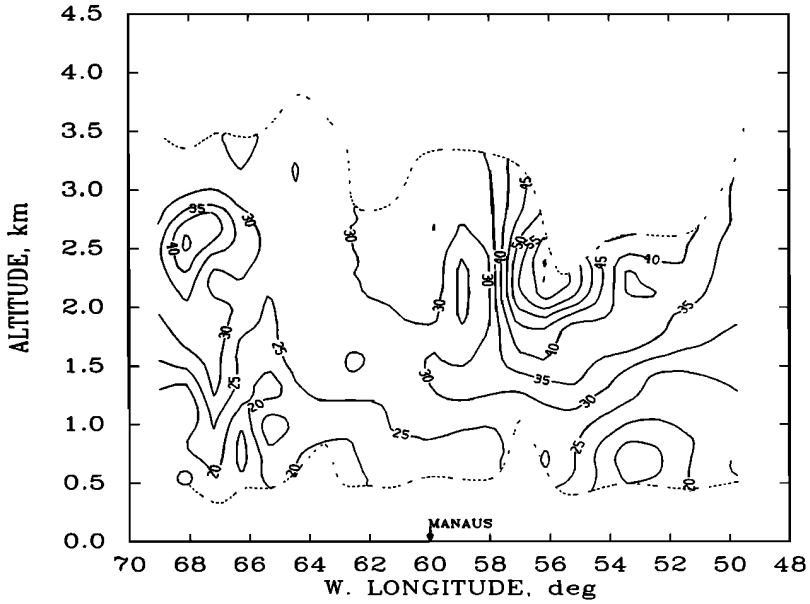

Fig. 8. Isopleths of O_3 mixing ratios across Amazon Basin generated from all average O_3 profiles obtained between August 5 and 8, 1985.

characteristics of O_3 associated with dry-season biomass burning will be amenable to satellite studies similar to those of *Fishman et al.* [1986]. The smaller-scale, more variable natural O_3 production and destruction processes in the ML will require further ground, aircraft, and photochemical-modeling studies.

CONCLUSIONS

Ozone and aerosol distributions were measured in the lower troposphere across the Amazon Basin during July–August 1985. Considerable spatial variation in O_3 and aerosol concentrations were observed on all long-range flights across the Basin. Positive and negative correlations between O_3 and aerosols were found in the PBL. The negative correlation results from the downward transport of relatively "clean," O_3-rich air from the upper troposphere into the PBL, which normally has higher aerosol loading and lower O_3 concentrations due to having an aerosol source and O_3 sink at the surface. Positive correlations between O_3 and aerosols are found in biomass-burning plumes, where the aerosols are directly emitted into the air and the O_3 is photochemically produced. Prior to the onset of the influence of biomass burning near Manaus, the daytime ML exhibited the largest amount of aerosol loading (0.25 cm^{-3} for aerosol diameters greater than 0.5 μm) with O_3 mixing ratios less than 20 ppbv. The PBL region between the ML and the TWI was observed to have 50% the aerosol loading of the ML and O_3 mixing ratios of 20–30 ppbv with a positive gradient of 2.8 ppbv km^{-1}. Immediately above the TWI, O_3 was found to increase rapidly at an average rate of about 10 ppbv km^{-1}, and the aerosol loading decreased to 40% of the PBL value. From ozonesonde data taken at Manaus, the O_3 mixing ratio was found to increase at an average rate of about 6 ppbv km^{-1} from the TWI to about 6 km ASL where the mixing ratio becomes nearly constant with altitude (Kirchhoff et al., submitted manuscript, 1987).

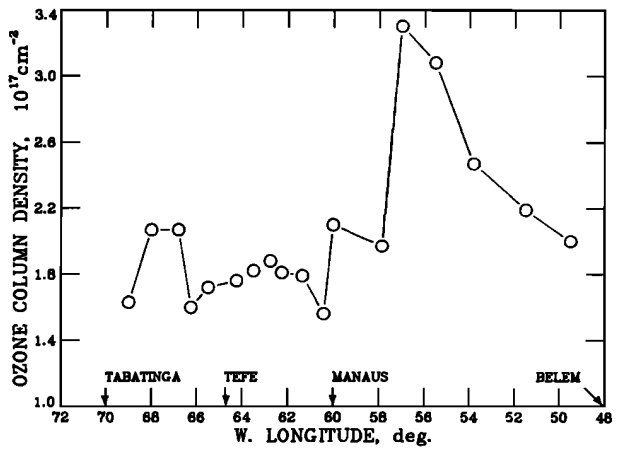

Fig. 9. Ozone column densities below trade wind inversion for August 5–9, 1985.

Structure of the atmosphere over the rain forest was determined from the contrast in aerosol lidar returns from the various air masses. Repeated observations of the ML permitted measurements of ML growth rate, which was found to be 7–10 cm s^{-1} in the late morning. The ML height typically did not exceed 1400 m AGL; however, the fair-weather convective clouds formed in the period from midmorning to late morning were found to routinely rise to the TWI where they were capped at about 3.1 km AGL. Because of inhomogeneity of the cloud activity in vertical and horizontal extent, the aerosol distribution between the ML and TWI is very inhomogeneous. This is also a "reservoir" region for plumes from biomass burning which are injected from the ML by buoyant forces in the heated plume and by cloud dynamics. Once material is deposited in this region, which is separated form the ML by a stable, narrow transition region at the top of the ML, it can be advected over long distances and can produce O_3 as a result of photochemical activity. Many layers of this type were observed during this field experiment, and their frequency and amount increased into the dry season.

On the survey flights between Manaus and Belem, it was found that the amount of O_3 increased by 59% over a 16-day period between July 23–24 and August 8–9. The eastern Amazon Basin was strongly influenced by transport of biomass-burning plumes from the south and southeast along a persistent anticyclonic circulation pattern. The O_3 mixing ratios were found to exceed 50 ppbv in many of these layers, which also had greatly enhanced aerosol loading and CO concentrations. Conditions to the west of Manaus were less affected by biomass burning because of the widespread persistence of rain over that area into early August. Localized cases of biomass burning along the Rio Solimões accounted for most of the excess O_3 found in the western Amazon Basin. This experiment has shown that a significant portion of the O_3 over the rain forest in the dry season is a result of biomass burning and that the distribution of photochemically produced O_3 is strongly affected by synoptic-scale transport from large fires to the south/southeast and from local production, primarily along the rivers.

Acknowledgments. The authors greatly appreciate the technical support of Carolyn Butler, Loyd Overbay, and Bill McCabe in operating the airborne DIAL system for the remote measurements of O_3 and aerosol profiles and that of Charles Hudgins in operating the airborne in situ systems for O_3 and aerosol measurements. We also thank Susan Kooi and Syed Ismail for their assistance in the DIAL O_3 data reduction and analysis. We appreciate the cooperation of the NASA Wallops Electra flight crew in conducting this demanding field experiment, and in particular, we recognize Roger Navarro, the aircraft coordinator, and John Riley and Bob Snell, the aircraft pilots. We also thank Susan Edwards for her help in preparing this manuscript.

REFERENCES

Ajtay, G. L., P. Ketner, and P. Duvigneaud, Terrestrial primary productivity and phytomass, in *The Global Carbon Cycle*, edited by B. Bolin et al., pp. 129–182, John Wiley, New York, 1979.

Andreae, M. O., et al., Biomass-burning emissions and associated haze layers over Amazonia, *J. Geophys. Res.*, this issue.

Browell, E. V., Remote sensing of tropospheric gases and aerosols with an airborne DIAL system, in *Optical Laser Remote Sensing*, edited by D. K. Killinger and A. Mooradian, pp. 138–147, Springer-Verlag, New York, 1983.

Browell, E. V., A. F. Carter, S. T. Shipley, R. J. Allen, C. F. Butler, M. N. Mayo, J. H. Siviter, Jr., and W. M. Hall, NASA multipurpose airborne DIAL system and measurements of ozone and aerosol profiles, *Appl. Opt.*, *22*, 522–534, 1983.

Browell, E. V., S. Ismail, and S. T. Shipley, Ultraviolet DIAL measurements of O_3 profiles in regions of spatially inhomogeneous aerosols, *Appl. Opt.*, *24*, 2827–2836, 1985*a*.

Browell, E. V., S. T. Shipley, C. F. Butler, and S. Ismail, Airborne lidar measurements of aerosols, mixed layer heights, and ozone during the 1980 PEPE/NEROS summer field experiment, *NASA Ref. Publ. RP-1143*, 1985*b*.

Browell, E. V., E. F. Danielsen, S. Ismail, G. L. Gregory, and S. M. Beck, Tropopause fold structure determined from airborne lidar and in situ measurements, *J. Geophys. Res.*, *92*, 2112–2120, 1987.

Ching, J. K. S., S. T. Shipley, and E. V. Browell, Evidence for cloud venting of mixed layer ozone, *Atmos. Environ.*, in press, 1987.

Crutzen, P. J., and L. T. Gidel, A two-dimensional photochemical model of the atmosphere, 2, The tropospheric budgets of the antropogenic chlorocarbons, CO, CH_4, CH_3Cl, and the effect of various sources of NO_x on tropospheric ozone, *J. Geophys. Res.*, *88*, 6641–6661, 1983.

Crutzen, P. J., L. E. Heidt, J. P. Krasnec, W. H. Pollock, and W. Seiler, Biomass burning as a source of atmospheric gases, CO, H_2, N_2O, NO, CH_3Cl, and COS, *Nature*, *282*, 253–256, 1979.

Crutzen, P. J., A. C. Delany, J. Greenberg, P. Haagenson, L. Heidt, R. Lueb, W. Pollock, W. Seiler, A. Wartburg, and P. Zimmerman, Tropospheric chemical composition measurements in Brazil during the dry season, *J. Atmos. Chem.*, *2*, 233–256, 1985.

Delany, A. C., P. J. Crutzen, P. Haagenson, S. Walters, and A. F. Wartburg, Photochemically produced ozone in the emissions from large-scale tropical vegetation fires, *J. Geophys. Res.*, *90*, 2425–2429, 1985.

Dickerson, R. R., Thunderstorms: An important mechanism in the transport of air pollutants, *Science*, *235*, 400–465, 1987.

Fishman, J., F. M. Vukovich, and E. V. Browell, The photochemistry of synoptic-scale ozone synthesis: Implications for the global tropospheric ozone budget, *J. Atmos. Chem.*, *3*, 299–320, 1985.

Fishman, J., P. Minnis, and H. G. Reichle, Jr., Use of satellite data to study tropospheric ozone in the tropics, *J. Geophys. Res.*, *91*, 14,451–14,465, 1986.

Garstang, M., et al., Trace gas exchanges and convective transports over the Amazonian rain forest, *J. Geophys. Res.*, this issue.

Gregory, G. L., C. H. Hudgins, and R. A. Edahl, Jr., Laboratory evaluation of an airborne ozone instrument which compensates for altitude/sensitivity effects, *Environ. Sci. Technol.*, *17*, 100–103, 1983.

Gregory, G. L., E. V. Browell, and L. S. Warren, Boundary layer ozone: An airborne survey above the Amazon Basin, *J. Geophys. Res.*, this issue.

Harriss, R. C., et al., The Amazon boundary layer experiment (ABLE 2A): Dry season 1985, *J. Geophys. Res.*, this issue.

Jacob, D. J., and S. C. Wofsy, Photochemistry of biogenic emissions over the Amazon forest, *J. Geophys. Res.*, this issue.

Kirchhoff, V. W. J. H., Surface ozone measurements in Amazonia, *J. Geophys. Res.*, this issue.

Martin, C. L., D. Fitzjarrald, M. Garstang, A. P. Oliveira, S. Greco, D. Martin, and E. Browell, Structure and growth of the mixing layer over the Amazonian rain forest, *J. Geophys. Res.*, this issue.

Reichle, H. G., Jr., V. S. Connors, J. A. Holland, W. D. Hypes, H. A. Wallio, J. C. Casas, B. B. Gormsen, M. S. Saylor, and W. D. Hesketh, Middle and upper tropospheric carbon monoxide mixing ratios as measured by a satellite-borne remote sensor during November 1981, *J. Geophys. Res.*, *91*, 10,865–10,887, 1986.

Sachse, G. W., R. C. Harriss, J. Fishman, G. F. Hill, and D. R. Cahoon, Carbon monoxide over the Amazon Basin during the 1985 dry season, *J. Geophys. Res.*, this issue.

Seiler, W., and P. J. Crutzen, Estimates of gross and net fluxes of carbon between the biosphere and the atmosphere from biomass burning, *Clim. Change*, *2*, 207–247, 1980.

Shipley, S. T., E. V. Browell, D. S. McDougal, B. L. Orndorff, and P. Haagenson, Airborne lidar observations of long-range transport in the free troposphere, *Environ. Sci. Technol.*, *18*, 749–756, 1984.

Torres, A. L., and H. Buchan, Tropospheric nitric oxide measurements over the Amazon Basin, *J. Geophys. Res.*, this issue.

Vukovich, F. M., J. Fishman, and E. V. Browell, The reservoir of ozone in the boundary layer of the eastern United States and its potential impact on the global tropospheric ozone budget, *J. Geophys. Res.*, *90*, 5687–5698, 1985.

E. V. Browell, Atmospheric Sciences Division, MS 401A, NASA Langley Research Center, Hampton, VA 23665.

G. L. Gregory and R. C. Harriss, Atmospheric Sciences Division, MS 483, NASA Langley Research Center, Hampton, VA 23665.

V. W. J. H. Kirchhoff, Instituto de Pesquisas Espaciais, 12201 São Jose dos Campos, São Paulo, Brazil.

(Received March 24, 1987;
revised August 5, 1987;
accepted August 26, 1987.)